ISSN-print: 2073-0764
ISSN-online: 2959-4340

TuJnaS

Thamar University Journal
of Natural & Applied Sciences

A peer-review Scientific Journal

Volume 8
Issue (1)
June 2023

Thamar University Publications

Thamar University Journal of

Natural and Applied Sciences (*TUJNAS*)

Thamar University Journal of Natural & Applied Sciences (*TUJNAS*) is published twice a year by Thamar University, Thamar, Yemen. It aims at publishing original research contributions covering pure science, Agriculture, Engineering, Medicine, Environment and Computer science.

✉ All correspondence should be sent to: ✉

Editorial Director,
Thamar University Journal of
Natural and Applied Sciences (TUJNAS)
Thamar University, P O Box: 87246 Dhamar, Republic of Yemen
E-mail: tujnas@tu.edu.ye

Volume (8), Issue (1) 2023

Editorial Board

Journal Website:
https://www.tu.edu.ye/journals/index.php/TUJNAS/index

Volume link:
https://www.tu.edu.ye/journals/index.php/TUJNAS/issue/view/127

TUJNAS
ISSN-Print: 2073-0764
ISSN-Online: 2959-4340

Thamar University Journal of Natural & Applied Sciences (TUJNAS)

Journal website:
www.tu.edu.ye/journals/index.php/TUJNAS/index

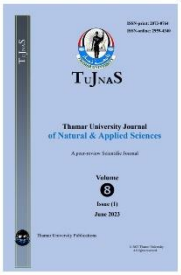

ORIGINAL ARTICLE

Partial Pre-Normality

Sadeq Ali Saad Thabit*

Affliations:
Department of Mathematics, Faculty of Education Almahra, Hadhramout University, Yemen

Corresponding Author:
Sadeq Ali Saad Thabit, Email: sthabit1975@gmail.com & sthabit1975@hu.edu.ye

Received: Mar 1, 2023,

Accepted Date: May 11, 2023,

Online Date: Jun 12, 2023

Published: Jun 13, 2023

DOI:
https://doi.org/10.59167/tujnas.v8i1.1485

Abstract

The main purpose of this paper is to study a new weaker version of pre-normality called partial pre-normality, which lies between almost pre-normality (resp. quasi pre-normality) and mild pre-normality. A space is called a partially pre-normal space if for any two disjoint closed subsets of , one of which is closed domain and the other is -closed, can be separated by two disjoint pre-open subsets. We investigate this property and present some examples to illustrate the relationships between partial pre-normality and other weaker kinds of both pre-normality and pre-regularity.

Keywords

Partially normal; Pre-normal; Almost pre-normal; Mildly pre-normal; Quasi pre-normal

1. Introduction

Throughout this paper, a space X always means a topological space on which no separation axioms are assumed, unless explicitly stated. The symbols $\mathbb{R}$, $\mathbb{Q}$ and $\mathbb{P}$ denote to the set of real, rational and irrational numbers, respectively. For a subset A of X, $X\backslash A$, $\overline{A}$ and $int(A)$ denote to the complement, the closure and the interior of A in X, respectively. A subset A of X is said to be a *regularly-open* set or an *open domain* set if it is the interior of its own closure, or equivalently if it is the interior of some closed set [1]. A complement of an open domain subset is called closed domain. A subset A of X is called a *π-closed* set if it is a finite intersection of closed domain sets [2]. A complement of a π-closed set is called *π-open*. Two sets A and B of X are said to be *separated* if there exist two disjoint open sets U and V in X such that $A \subseteq U$ and $B \subseteq V$ [3,4,5]. A subset A of X is said to be a *pre-open* set [6] if $A \subseteq int(\overline{A})$. A subset A of X is said to be *semi open* if $A \subseteq \overline{int(A)}$ [7]. A subset A of X is called *α-open* if $A \subseteq int(\overline{int(A)})$ [8]. A space X is called a *pre-normal* space [9] if any two disjoint closed subsets A and B of X can be separated by two disjoint pre-open subsets. A space X is called an *almost pre-normal* space [8] if any two disjoint closed subsets A and B of X, one of which is closed domain, can be separated by two disjoint pre-open subsets. A space X is called a *mildly pre-normal* space [8] if any pair of disjoint closed domain subsets A and B of X, can be separated by two disjoint pre-open subsets. A space X is said to be a *partially normal* space [10] if any pair of disjoint closed subsets A and B of X, one of which is π-closed and the other is closed domain, can be separated by two disjoint open subsets. A space X is said to be a *π-pre-normal* (or πp-normal) space [11] if any pair of disjoint closed subsets A and B of X, one of which is π-closed, can be separated by two disjoint pre-open subsets. A complement of a pre-open (resp. semi open, α-open) set is called pre-closed (resp. semi closed, α-closed). An intersection of all pre-closed sets containing A is called *pre-closure* of A [12] and denoted by $p\ cl(A)$. A *pre-interior* of A denoted by $p\ int(A)$, is defined to be the union of all pre-open sets contained in A.

In this paper, we study a new weaker version of pre-normality called partial pre-normality. We show that partial pre-normality is both an additive and a topological property, and it is a hereditary property only with respect to closed domain subspaces. Some properties, examples, characterizations and preservation theorems of partial pre-normality are presented in this work.

2. Definition and Examples

First, we give the definition of partial pre-normality.

Definition 2.1 A space X is said to be a *partially pre-normal* space if for every pair of disjoint closed subsets A and B of X, one of which is π-closed and the other is closed domain, there exist disjoint pre-open subsets U and V of X such that $A \subseteq U$ and $B \subseteq V$.

It can be observed that every partially normal space is partially pre-normal because every open set is pre-open, and we conclude:

pre-normal $\Longrightarrow$ almost pre-normal $\Longrightarrow$ partially pre-normal $\Longrightarrow$ mildly pre-normal

pre-normal $\Longrightarrow$ quasi pre-normal $\Longrightarrow$ partially pre-normal $\Longrightarrow$ mildly pre-normal

Some counterexamples will be given in this paper to show that none of the above implications is reversible. First, we need to recall the following definition:

Definition 2.2 A space X is called a *sub-maximal* space [13,14] if every dense subset of X is an open subset.

Note that: every pre-open subset in a sub-maximal space X is an open subset. The following facts have been presented in [15] (Chapter 7).

Lemma 2.3 Let X be a space and D be a dense subset of X, then::

1. D is pre-open set in X.
2. for any subset A of X, we have $A \cup D$ is a pre-open subset.
3. for any closed subset A of X, we have $D \backslash A$ is a pre-open subset.
4. if A and B are disjoint closed subsets of X, then $(D \backslash A) \cup B$ and $(D \backslash B) \cup A$ are pre-open.
5. if X has two disjoint dense subsets, then X is pre-normal space.

Since every pre-open subset in a sub-maximal space is an open subset, we get:

Lemma 2.4 Every partially pre-normal sub-maximal space is partially normal.

Here is an example of a mildly pre-normal space but not partially pre-normal.

Example 2.5 *The irregular lattice topology* , Example 79 in [16]:

Let $X = \{(i,k): i,k \in \mathbb{Z}, i,k > 0\} \cup \{(i,0);\ i \geq 0\}$ be the subset of the integral lattice points of the plane. The irregular lattice topology on X is Urysohn, σ-compact, Lindelöf, second countable, not semi regular and has σ-locally finite base [16]. It is easy to show that the irregular lattice topology is a sub-maximal space because any dense subset of X is an open subset. Hence, every pre-open set in X is an open subset. The irregular lattice topology is a mildly normal space but not partially normal [10]. Thus, it is a mildly pre-normal space. Since X is sub-maximal non partially normal, by the Lemma 2.4 we obtain X is not partially pre-normal space.

The following is an example of a partially pre-normal space but not almost pre-normal.

Example 2.6 *The countable complement extension topology* , Example 63 in [16]:

Let $X = \mathbb{R}$ and let $\mathcal{T}_1 = \mathcal{U}$ the Euclidean topology on $\mathbb{R}$. Let $\mathcal{T}_2 = \mathcal{CC}$ the co-countable topology on $\mathbb{R}$. Define $\mathcal{T}$ to be the smallest topology generated by $\mathcal{T}_1 \cup \mathcal{T}_2$, which is called a *countable complement extension* topology on X [16]. In this space, the only open domain (closed domain, π-open, π-closed) sets in $(X,\mathcal{T})$ are those which are open domain (closed domain, π-open, π-closed) in $(\mathbb{R},\mathcal{U})$, where $\mathcal{U}$ is the Euclidean topology on $\mathbb{R}$. It can be observed that: $(X,\mathcal{T})$ is almost regular, Lindelöf, not almost normal, not semi-regular and $\mathbb{P}$ is open. For more information about this space, see [15, 16]. Note that: in the countable complement extension topology, we have $\mathbb{P}$ is dense open subspace and any uncountable subset of $\mathbb{P}$ whose complement is countable, is also open set in X. Thus, we can easily show that any dense subset of X is an open set in X. Therefore, X is a sub-maximal space. Hence, every pre-open subset of X is an open subset. Since every almost regular Lindelöf space is quasi-normal [17], we have X is a quasi-normal space and hence partially normal. Therefore, the countable complement extension topology is a partially pre-normal space. Since X is sub-maximal non almost normal space, we obtain that X is not almost pre-normal. Hence, the countable complement extension topology is an example of a partially pre-normal space but not almost pre-normal.

Every partially normal space is partially pre-normal but the converse is not true in general as shown by the following example:

Example 2..7 Consider the product space $X = (\omega_0 + 1) \times [-1,1]$, where ω_0 is the first countable ordinal. Let $p = (\omega_0, 0) \in X$, define a topology on X by adding to the product

topology of X, the basic open set of p which is the form $U_n(p) = \{p\} \cup ((\alpha, \omega_0] \times (0, \frac{1}{n})), n \in \mathbb{N}$, $\alpha < \omega_0$. Now, we show that X is partially pre-normal but not partially normal. To prove the space X is partially pre-normal, let A be π-closed and B be closed domain sets in X such that $A \cap B = \emptyset$. Let $G = \omega_0 + 1 \times ((-1,1) \cap \mathbb{Q})$ and $H = \omega_0 + 1 \times ((-1,1) \cap \mathbb{P})$. Then, G and H are disjoint dense subsets of X. Let $U = G \cup A$ and $V = H \cup B$. By the Lemma 2.3, we have U and V are disjoint pre-open sets in X such that $A \subseteq U$ and $B \subseteq V$. Thus, A and B can be separated by two disjoint pre-open subsets. Hence, X is partially pre-normal. Now, we show that X is not partially normal. Let $U = \{1,3,5, \dots\} \times [-1,0)$ and $V = \{0,2,4,6, \dots\} \times (0,1]$. Then, U and V are open sets in X such that $\overline{U} = (U \cup \{\omega_0\}) \times [-1,0] \backslash \{(\omega_0, 0)\}$ and $\overline{V} = (V \cup \{\omega_0\}) \times [0,1]$. Let $E = \overline{U}$ and $F = \overline{V}$. Then, E and F are disjoint closed domain sets in X. But E and F can not be separated by two disjoint open subsets. Hence, X is not mildly normal space and hence not partially normal. Therefore, the space X is an example of a partially pre-normal space but not partially normal.

The following example is a partially pre-normal space but not pre-normal.

Example 2.8 Consider the topology $\mathcal{T} = \{X, \emptyset, \{a\}, \{a, b\}, \{a, c\}\}$ on the set $X = \{a, b, c\}$. Then, X is almost pre-normal [11]. Hence, it is partially pre-normal. But X is not pre-normal because the sets $\{b\}$ and $\{c\}$ are disjoint closed subsets of X and they can not be separated by two disjoint pre-open subsets. So, $(X, \mathcal{T})$ is an example of a partially pre-normal space but not pre-normal.

Example 2.9 *The simplified arens square topology*, Example 81 in [16], is Hausdorff, not completely Hausdorff (not Urysohn), semi regular, not regular, not normal, Lindelöf, σ-compact and with σ-locally finite base [16]. Since X is semi regular and not regular space, we get X is not almost regular. Since X is T_1 and not almost regular space, we have X is not almost normal. But X is quasi normal space [18]. Thus, it is a partially normal space and hence partially pre-normal. Since S is an open dense subspace of X, the sets $C = S \cap \mathbb{Q}$ and $D = S \cap \mathbb{P}$ are disjoint dense subsets of X. Therefore, X is a pre-normal space. Therefore, the simplified arens square topology is an example of a partially pre-normal space but not almost regular. Note that X is a pre-regular space but not regular.

3. Characterizations of Partial Pre-normality

Now, we give some characterizations of partial pre-normality.

Theorem 3.1 For a space X, the following statements are equivalent:

(a). X is partially pre-normal.

(b). for every pair of open sets U and V, one of which is open domain and the other is π-open whose union is X, there exist pre-closed subsets G and H of X such that $G \subseteq U$, $H \subseteq V$ and $G \cup H = X$.

(c). for any π-closed set A and each open domain set B such that $A \subseteq B$, there exists pre-open set U such that $A \subseteq U \subseteq p\ cl(U) \subseteq B$.

(d). for every closed domain set A and each π-open set B such that $A \subseteq B$, there exists a pre-open set U such that $A \subseteq U \subseteq p\ cl(U) \subseteq B$.

(e). for every pair of disjoint closed sets A and B of X, one of which is closed domain and the other is π-closed, there exist two pre-open subsets U and V of X such that $A \subseteq U$, $B \subseteq V$ and $p\ cl(U) \cap p\ cl(V) = \emptyset$.

Proof. $(a) \Longrightarrow (b)$. Let U be an open domain subset and V be a π-open subset of a partially pre-normal space X such that $U \cup V = X$. Then, $X\backslash U$ and $X\backslash V$ are disjoint, where $X\backslash U$ is closed domain and $X\backslash V$ is π-closed. By partial pre-normality of X, there exist disjoint pre-open subsets U_1 and V_1 of X such that $X\backslash U \subseteq U_1$ and $X\backslash V \subseteq V_1$. Let $G = X\backslash U_1$ and $H = X\backslash V_1$. Thus, G and H are pre-closed subsets of X such that $G \subseteq U$, $H \subseteq V$ and $G \cup H = X$.

$(b) \Longrightarrow (c)$. Let A be a π-closed and B be an open domain subset such that $A \subseteq B$. Then, $X\backslash A$ is π-open and B is open domain in X whose union is X. Then by (b), there exist pre-closed sets G and H such that $G \subseteq X\backslash A$, $H \subseteq B$ and $G \cup H = X$. So, $A \subseteq X\backslash G$, $X\backslash B \subseteq X\backslash H$ and $(X\backslash G) \cap (X\backslash H) = \emptyset$. Let $U = X\backslash G$ and $V = X\backslash H$. Then, U and V are disjoint pre-open sets such that $A \subseteq U \subseteq X\backslash V \subseteq B$. Since $X\backslash V$ is pre-closed, we have $p\ cl(U) \subseteq X\backslash V$. Thus, $A \subseteq U \subseteq p\ cl(U) \subseteq B$.

$(c) \Longrightarrow (d)$. Let A be closed domain and B be π-open sets in X such that $A \subseteq B$. Then, $X\backslash B \subseteq X\backslash A$, where $X\backslash B$ is π-closed and $X\backslash A$ is open domain. By (c), there exists a pre-open set V such that $X\backslash B \subseteq V \subseteq p\ cl(V) \subseteq X\backslash A$. This implies that $A \subseteq X\backslash p\ cl(V) \subseteq X\backslash V \subseteq B$. Put $U = X\backslash p\ cl(V)$. Then, U is a pre-open set in X such that $A \subseteq U \subseteq p\ cl(U) \subseteq B$.

$(d) \Longrightarrow (e)$. Let A and B be any disjoint closed sets such that A is closed domain and B is π-closed. Then, $A \subseteq X\backslash B$, where $X\backslash B$ is π-open. By (d), there exists a pre-open subset U of X such that $A \subseteq U \subseteq p\ cl(U) \subseteq X\backslash B$. Thus, we have $B \subseteq X\backslash p\ cl(U)$. Let $V = X\backslash p\ cl(U)$. Thus, V is a pre-open subset of X. Therefore, there exist two pre-open subsets U and V such that $A \subseteq U$, $B \subseteq V$ and $p\ cl(U) \cap p\ cl(V) = \emptyset$.

$(e) \Longrightarrow (a)$. It is obvious.

4. Partial Pre-normality in Subjects

The following two lemmas have been presented in [11, 15, 19].

Lemma 4.1 Let $f: X \to Y$ be a function. Then:

1. an image of a pre-open set under an open continuous function is pre-open.

2. an image of a pre-closed set under an onto, open-and-closed (clopen) continuous function is pre-closed.

3. an inverse image of a pre-open (resp. pre-closed, π-open, π-closed) set under an open continuous function is pre-open (resp. pre-closed, π-open, π-closed).

Lemma 4.2 Let M be a closed domain (resp. open, dense) subspace of X and $A \subseteq X$. If A is a pre-open (resp. pre-closed) set in X, then $A \cap M$ is a pre-open (resp. pre-closed) set in M.

Theorem 4.3 An image of a partially pre-normal space under an open continuous injective function is partially pre-normal.

Proof. Let X be a partially pre-normal space and let $f: X \longrightarrow Y$ be an open continuous injective function. We show that $f(X)$ is partially pre-normal. Let A and B be any two disjoint closed sets in $f(X)$, one of which is π-closed and the other is closed domain. Since the inverse image of a π-closed (closed domain) set under an open continuous function is π-closed (closed domain), by the Lemma 4.1, we have $f^{-1}(A)$ is π-closed in X, $f^{-1}(B)$ is closed domain in X and $f^{-1}(A) \cap f^{-1}(B) = \emptyset$. By partial pre-normality of X, there exist two pre-open subsets U and V of X such that $f^{-1}(A) \subseteq U$, $f^{-1}(B) \subseteq V$ and $U \cap V = \emptyset$. Since f is an open continuous injective function, we have $A \subseteq f(U)$, $B \subseteq f(V)$ and $f(U) \cap f(V) = \emptyset$. By the Lemma 4.1, we obtain $f(U)$ and $f(V)$ are disjoint pre-open sets in $f(X)$ such that $A \subseteq f(U)$ and $B \subseteq f(V)$. Hence, $f(X)$ is partially pre-normal.

From the Theorem 4.3, we obtain:

Corollary 4.4 Partial pre-normality is a topological property.

Theorem 4.5 Partial pre-normality is a hereditary property with respect to closed domain subspaces.

Proof. Let M be a closed domain subspace of a partially pre-normal space X. Let A and B be any disjoint closed sets such that A is π-closed and B is closed domain in M. Since M is a closed domain subspace of X, we have A and B are disjoint closed subsets of X, where A is π-closed and B is closed domain. By partial pre-normality of X, there exist two disjoint pre-open subsets U and V of X such that $A \subseteq U$ and $B \subseteq V$. By the Lemma 4.2, we obtain $U \cap M$ and $V \cap M$ are disjoint pre-open sets in M such that $A \subseteq U \cap M$ and $B \subseteq V \cap M$. Hence, M is partially pre-normal.

Since every closed-and-open (clopen) subset is closed domain, we have:

Corollary 4.6 Partial pre-normality is a hereditary property with respect to clopen subspaces.

5. Relationships of Partial Pre-normality

In this section, we present some relationships between partial pre-normality and almost pre-regularity. First, we recall the following definitions:

Definition 5.1 A space X is called an *almost pre-regular* space if for each closed domain set F and each $x \notin F$, there exist disjoint pre-open sets U and V such that $x \in U$ and $F \subseteq V$ [6,12].

Definition 5.2 A space X is called a *weakly pre-regular* space [8] if for each $x \in X$ and for each open domain subset U of X such that $x \in U$, there exists a pre-open subset V of X such that $x \in V \subseteq p\,cl(V) \subseteq U$.

Partial pre-normality does not imply to almost pre-regularity in general as shown by the following example.

Example 5.3 Consider the topology $\mathcal{T} = \{X, \emptyset, \{a\}, \{b\}, \{a, b\}\}$ on the set $X = \{a, b, c\}$ [11], we have X is pre-normal and hence partially pre-normal space. But X is not almost pre-regular because the closed domain $\{a, c\}$ does not contain the point b, and they do not exist two disjoint

pre-open subsets containing them. So, $(X, \mathcal{T})$ is an example of a partially pre-normal space but not almost pre-regular.

Definition 5.4 A space X is called a p_1-*paracompact* space [6,20] if every pre-open cover of X has a locally finite pre-open refinement.

Clearly, every p_1-paracompact space is nearly paracompact. The following result is analogous to the Theorem 5.5 in [8].

Theorem 5.5 Every weakly pre-regular p_1-paracompact space is partially pre-normal.

Proof. Let X be a weakly pre-regular p_1-paracompact space. Since X is p_1-paracompact, it is sub-maximal and nearly paracompact, Theorem 1 in [21]. Since X is a sub-maximal and a weakly pre-regular space, it is weakly regular. In view of that fact that every weakly regular nearly paracompact space is π-normal [15], we obtain X is partially normal. Hence, X is partially pre-normal.

Since every almost pre-regular space is weakly pre-regular, we get:

Corollary 5.6 Every almost pre-regular p_1-paracompact space is partially pre-normal.

It can be observed that: partial pre-normality does not imply to almost regularity and vise versa. The simplified arens square topology, Example 2.9 is a partially normal T_1-space but not almost regular. Thus, it is partially pre-normal T_1-space but not almost regular.

Theorem 5.7 Every partially pre-normal T_1-space in which every singleton $\{x\}$ is π-closed is almost pre-regular.

Proof. It is obvious.

6. Properties of Partial Pre-normality

Now, we present the following result which is in [15].

Corollary 6.1 If $A \subseteq X = \bigoplus_{s\in S} X_s$ is π-open (resp. π-closed) in X, then $A \cap X_s$ is π-open (resp. π-closed) in X_s for each $s \in S$.

Theorem 6.2 The sum $X = \bigoplus_{s\in S} X_s,\ X_s \neq \emptyset\ \forall\ s \in S$ is partially pre-normal if and only if each X_s is partially pre-normal for each $s \in S$.

Proof. Let $X = \bigoplus_{s\in S} X_s$ be a partially pre-normal space. Since X_s is a clopen subset of X, by the Corollary 4.6 we have X_s is a partially pre-normal subspace of X for each $s \in S$. Conversely, suppose that X_s is partially pre-normal for each $s \in S$. We show that X is partially pre-normal. Let A and B be any two disjoint closed subsets of X such that A is π-closed and B is closed domain. Thus, we have $A \cap X_s$ is π-closed and $B \cap X_s$ is closed domain in X_s for each s. Since $A \cap B = \emptyset$, we have $(A \cap X_s) \cap (B \cap X_s) = \emptyset$. Since X_s is partially pre-normal for each s, there exist pre-open sets U_s and V_s in X_s such that $A \cap X_s \subseteq U_s$, $B \cap X_s \subseteq V_s$ and $U_s \cap V_s = \emptyset$. Now, since $\{X_s : s \in S\}$ is a family of pairwise disjoint topological spaces, we get $A = \cup_{s\in S} (A \cap X_s) \subseteq \cup_{s\in S} U_s = U$, $B = \cup_{s\in S} (B \cap X_s) \subseteq \cup_{s\in S} V_s = V$ and $U \cap V = (\cup_{s\in S} U_s) \cap (\cup_{s\in S} V_s) = \cup_{s\in S} (U_s \cap V_s) = \emptyset$. Thus, U and V are disjoint pre-open sets in X such that $A \subseteq U$ and $B \subseteq V$. Therefore, X is partially pre-normal.

Corollary 6.3 Partial pre-normality is an additive property.

It is well known that, a finite product of pre-open (pre-closed) sets is pre-open (pre-closed) [15]. So, we get:

Theorem 6.4 Let $(X_i, \mathcal{T}_i)$ be a space, $i = 1,2,3, \dots, n$. If $X = \prod_{i=1}^{n} X_i$ is partially pre-normal, then $(X_i, \mathcal{T}_i)$ is partially pre-normal for each $i = 1,2,3, \dots, n$.

Proof. Let $X = \prod_{i=1}^{n} X_i$ be partially pre-normal. Let $m \in \{1,2,3, \dots, n\}$ be arbitrary. Let A and B be any two disjoint closed sets in X_m, where A is π-closed and B is closed domain. Let $\pi_m : \prod_{i=1}^{n} X_i \longrightarrow X_m$ be the natural projection map from X onto X_m. Now, $\pi_m^{-1}(A) = \prod_{i=1}^{n} W_i$, (where $W_i = X_i$ for each $i \neq m$) is π-closed in X, $\pi_m^{-1}(B) = \prod_{i=1}^{n} V_i$, (where $V_i = X_i$ for each $i \neq m$) is closed domain in X and $\pi_m^{-1}(A) \cap \pi_m^{-1}(B) = \emptyset$. Since X is partially pre-normal, there exist two disjoint pre-open sets U and V in X such that $\pi_m^{-1}(A) \subseteq U$ and $\pi_m^{-1}(B) \subseteq V$. Since π_m is an open onto continuous function, by the Lemma 4.1 $\pi_m(U)$ and $\pi_m(V)$ are disjoint pre-open subsets of X_m such that $A \subseteq \pi_m(U)$ and $B \subseteq \pi_m(V)$. Hence, X_m is partially pre-normal. Since m was arbitrary, we get $(X_i, \mathcal{T}_i)$ is partially pre-normal for each $i \in \{1,2,3, \dots, n\}$.

7. Other Characterizations of Partial Pre-normality

Now, we need to recall the following definitions.

Definition 7.1 A subset A of a space X is called:

1. *g-closed* (resp. *g-open*) [21] if $\overline{A} \subseteq U$ whenever $A \subseteq U$ and U is open (resp. if $F \subseteq \mathrm{int}(A)$ whenever $F \subseteq A$ and F is closed).

2. *g^*-closed* (resp. *g^*-open*) [22], if $\overline{A} \subseteq U$ whenever $A \subseteq U$ and U is g-open (resp. if $F \subseteq \mathrm{int}(A)$ whenever $F \subseteq A$ and F is g-closed).

3. *πg-closed* (resp. *πg-open*) [23] if $\overline{A} \subseteq U$ whenever $A \subseteq U$ and U is π-open (resp. if $F \subseteq \mathrm{int}(A)$ whenever $F \subseteq A$ and F is π-closed).

4. *gp-closed* (resp. *gp-open*) [24] if $p\ \mathrm{cl}(A) \subseteq U$, whenever $A \subseteq U$ and U is open (resp. if $F \subseteq p\ \mathrm{int}(A)$, whenever $F \subseteq A$ and F is closed).

5. *g^*p-closed* (resp. *g^*p-open*) [25] if $p\ \mathrm{cl}(A) \subseteq U$ whenever $A \subseteq U$ and U is g-open (resp. if $F \subseteq p\ \mathrm{int}(A)$, whenever $F \subseteq A$ and F is g-closed).

6. *πgp-closed* (resp. *πgp-open*) [26] if $p\ \mathrm{cl}(A) \subseteq U$ whenever $A \subseteq U$ and U is π-open (resp. if $F \subseteq p\ \mathrm{int}(A)$, whenever $F \subseteq A$ and F is π-closed).

7. *rgp-closed* (resp. *rgp-open*) [14] if and only if $\mathrm{cl}(A) \subseteq U$ whenever $A \subseteq U$ and U is an open domain (resp. if and only if $F \subseteq p\ \mathrm{int}(A)$, whenever $F \subseteq A$ and F is a closed domain).

From the Definition 7.1, we have:

closed $\Longrightarrow$ g^*-closed $\Longrightarrow$ g-closed $\Longrightarrow$ πg-closed $\Longrightarrow$ rg-closed

closed $\Longrightarrow$ pre-closed $\Longrightarrow$ g^*p-closed $\Longrightarrow$ gp-closed $\Longrightarrow$ πgp-closed $\Longrightarrow$ rgp-closed

The following theorem gives some other characterizations of partial pre-normality.

Theorem 7.2 For a space X, the following are equivalent:

(a). X is partially pre-normal.

(b). for each π-closed set A and each closed domain set B such that $A \cap B = \emptyset$, there exist disjoint g^*p-open (resp. gp-open, πgp-open, rgp-open) subsets U and V of X such that $A \subseteq U$ and $B \subseteq V$.

(c) . for any π-closed set A and any open domain set B with $A \subseteq B$, there exists a g^*p-open (resp. gp-open, πgp-open, rgp-open) subset V of X such that $A \subseteq V \subseteq p\ cl(V) \subseteq B$.

(d). for any closed domain set A and each π-open set B with $A \subseteq B$, there exists a g^*p-open (resp. gp-open, πgp-open, rgp-open) subset V of X such that $A \subseteq V \subseteq p\ cl(V) \subseteq B$.

Proof. $(a) \Longrightarrow (b)$. Let X be a partially pre-normal space. Let A be π-closed and B be closed domain such that $A \cap B = \emptyset$. By partial pre-normality of X, there exist disjoint pre-open subsets U and V of X such that $A \subseteq U$ and $B \subseteq V$. Thus, U and V are disjoint g^*p-open (resp. gp-open, πgp-open, rgp-open) subsets of X such that $A \subseteq U$ and $B \subseteq V$.

$(b) \Longrightarrow (c)$. Suppose (b) holds. Let A be π-closed and B be an open domain subset of X such that $A \subseteq B$. Then, $A \cap X\backslash B = \emptyset$. Thus, A and $X\backslash B$ are disjoint, where A is π-closed and $X\backslash B$ is closed domain. By (b), there exists disjoint rgp-open subsets U and V of X such that $A \subseteq U$ and $X\backslash B \subseteq V$. Therefore, we have $A \subseteq p\ int(U)$, $X\backslash B \subseteq p\ int(V)$ and $p\ int(U) \cap p\ int(V) = \emptyset$. Let $G = p\ int(U)$. Then, G is a pre-open subset of X and hence g^*p-open (resp. gp-open, πgp-open, rgp-open) such that $A \subseteq G \subseteq p\ cl(G) \subseteq B$.

$(c) \Longrightarrow (d)$. Suppose (c) holds. Let A be closed domain and B be π-open subsets of X such that $A \subseteq B$. Then, $X\backslash B \subseteq X\backslash A$, where $X\backslash B$ is π-closed and $X\backslash A$ is open domain. By (c), there exists πgp-open set U such that $X\backslash B \subseteq U \subseteq cl(U) \subseteq X\backslash A$. This implies that $X\backslash B \subseteq pint(U) \subseteq pint(pcl(U) \subseteq pcl(U) \subseteq X\backslash A$. Thus, we have $A \subseteq X\backslash pcl(U) \subseteq X\backslash pint(pcl(U)) \subseteq X\backslash pint(U) \subseteq B$. Put $V = X\backslash pcl(U)$. Then, V is pre-open and hence a g^*p-open (resp. gp-open, πgp-open, rgp-open) subset of X such that $A \subseteq V \subseteq pcl(V) \subseteq B$.

$(d) \Longrightarrow (a)$. Suppose (d) holds. Let A be closed domain and B be π-closed such that $A \cap B = \emptyset$. Then, we have $A \subseteq X\backslash B$ where $X\backslash B$ is π-open. By (d), there exists an rgp-open subset V of X such that $A \subseteq V \subseteq p\ cl(V) \subseteq X\backslash B$. Then, we obtain $A \subseteq p\ int(V) \subseteq V \subseteq p\ cl(V) \subseteq X\backslash B$. Let $G = p\ int(V)$ and $H = X\backslash p\ cl(V)$. Then, G and H are disjoint pre-open subsets of X such that $A \subseteq G$ and $B \subseteq H$. Hence, X is partially pre-normal.

8. Preservation Theorems on Partial Pre-normality

In this section, we present some preservation theorems of partial pre-normality. First, recall the following definitions:

Definition 8.1 A function $f: X \longrightarrow Y$ is said to be:

1. *rc-continuous* [27] if $f^{-1}(F)$ is closed domain in X for each closed domain F of Y.

2. *π-continuous* [23,28] if $f^{-1}(F)$ is π-closed in X for each closed F of Y.

3. *weakly open* [14] if for each open subset U of X, $f(U) \subseteq \text{int}(f(\overline{U}))$.

4. *R-map* [14,23] if $f^{-1}(V)$ is open domain in X for every open domain set V of Y.

5. *almost pre-irresolute* [29] if for each $x \in X$ and each pre-neighborhood V of $f(x)$ in Y, $p\ cl(f^{-1}(V))$ is a pre-neighborhood of x in X.

6. *Mp-closed* (resp. *Mp-open*) [6,12,14] if $f(U)$ is pre-closed (resp. pre-open) in Y for each pre-closed (resp. pre-open) U in X.

Lemma 8. 2, [14], If $f: X \longrightarrow Y$ is a weakly open continuous function, then f is Mp-open and R-map.

Clearly, every pre-irresolute function is almost pre-irresolute, and every π-continuous function is continuous. Now, we present the following preservation theorems of partial pre-normality.

Theorem 8.3 If $: X \longrightarrow Y$ is an Mp-open rc-continuous and almost pre-irresolute surjection function from a partially pre-normal space X onto a space Y, then Y is partially pre-normal.

Proof. Let A be a π-closed and B be an open domain subsets of Y such that $A \subseteq B$. Then by rc-continuity of f, $f^{-1}(A)$ is π-closed and $f^{-1}(B)$ is open domain subsets of X such that $f^{-1}(A) \subseteq f^{-1}(B)$. Since X is partially pre-normal, by the Theorem 3.1, there exists a pre-open subset V of X such that $f^{-1}(A) \subseteq V \subseteq p\ cl(V) \subseteq f^{-1}(B)$. Since f is Mp-open and almost pre-irresolute surjection, it follows that $f(V)$ is a pre-open subset of Y and $A \subseteq f(V) \subseteq p\ cl(f(V)) \subseteq B$. By the Theorem 3.1, we obtain Y is partially pre-normal.

Theorem 8.4 If $: X \longrightarrow Y$ is an Mp-open, open, π-continuous and almost pre-irresolute function from a partially pre-normal space X onto a space Y, then Y is partially pre-normal.

Proof. Let A be π-closed in Y and B be open domain in Y such that $A \subseteq B$. By π-continuity and openness of f, $f^{-1}(A)$ is π-closed and $f^{-1}(B)$ is open domain in X such that $f^{-1}(A) \subseteq f^{-1}(B)$. By partially pre-normality of X, there exists a pre-open set U of X such that $f^{-1}(A) \subseteq U \subseteq p\ cl(U) \subseteq f^{-1}(B)$. Since f is Mp-open almost pre-irresolute surjection, we obtain $A \subseteq$

$f(U) \subseteq p\ cl(f(U)) \subseteq B$, where $f(U)$ is pre-open in Y. By the Theorem 7.2, we get Y is partially pre-normal.

Theorem 8.5 If : $X \longrightarrow Y$ is an Mp-closed and open π-continuous function from a partially pre-normal space X onto a space Y, then Y is partially pre-normal.

Proof. Let U and V be open subsets of Y such that U is π-open and V is open domain such that $U \cup V = Y$. This implies that $f^{-1}(U) \cup f^{-1}(V) = X$. By openness π-continuity of f, $f^{-1}(U)$ is π-open in X and $f^{-1}(V)$ is open domain in X. Since X is partially pre-normal, by the Theorem 3.1 there exist pre-closed sets G and H in X such that $G \subseteq f^{-1}(U)$, $H \subseteq f^{-1}(V)$ and $G \cup H = X$. Thus, $f(G) \subseteq U$, $f(H) \subseteq V$ and $f(G) \cup f(H) = Y$. Since f is an Mp-closed function, we have $f(G)$ and $f(H)$ are pre-closed subsets of Y. By the Theorem 3.1, we obtain Y is partially pre-normal.

Theorem 8.6 If $f: X \longrightarrow Y$ is an open π-continuous, weakly open surjection and X is partially pre-normal, then Y is partially pre normal.

Proof. Let A and B be any disjoint closed subsets of Y such that A is π-closed and B is closed domain. Since f is an open π-continuous surjection, we have $f^{-1}(A)$ and $f^{-1}(B)$ are disjoint, $f^{-1}(A)$ is π-closed and $f^{-1}(B)$ is closed domain subsets of X. Since X is partially pre-normal, there exist disjoint pre-open sets U and V in X such that $f^{-1}(A) \subseteq U$ and $f^{-1}(B) \subseteq V$. Since f is a weakly open continuous surjection, by the Lemma 8.2, we have f is Mp-open and R-map. Thus, $f(U)$ and $f(V)$ are disjoint pre-open sets in Y such that $A \subseteq f(U)$ and $B \subseteq f(V)$. Hence, Y is partially pre-normal.

Theorem 8.7 If $f: X \longrightarrow Y$ is an Mp-open, rc-continuous and almost pre-irresolute surjection on a partially pre-normal space X onto a space Y, then Y is partially pre-normal.

Proof. Let A be π-closed and B be open domain in Y such that $A \subseteq B$. By rc-continuity of f, we obtain $f^{-1}(A)$ is π-closed in X and $f^{-1}(B)$ is open domain in X such that $f^{-1}(A) \subseteq f^{-1}(B)$. By partial pre-normality of X, there exists a pre-open set U such that $f^{-1}(A) \subseteq U \subseteq p\ cl(U) \subseteq f^{-1}(B)$. Thus, $f(f^{-1}(A)) \subseteq f(U) \subseteq f(p\ cl(U)) \subseteq f(f^{-1}(B))$. Since f is an Mp-

open, almost pre-irresolute surjection, we obtain $A \subseteq f(U) \subseteq p\ cl(f(U)) \subseteq B$, where $f(U)$ is a pre-open subset of Y. By the Theorem 3.1, we have Y is partially pre-normal.

We can distinguish some other preservation theorems on partial pre-normality similar to those on mild pre-normality, almost pre-normality and quasi pre-normality in [8,11].

Problems: The following problems are still open in this work.

1. Is there a T_1-space X that is a partially pre-normal space but not almost pre-regular?
2. Is there an example of a partially pre-normal space but not quasi pre-normal?

9. Conclusions

A new version of pre-normality called partial pre-normality have been studied in this work. We have shown that partial pre-normality is both a topological and an additive property, and it is a hereditary property with respect to closed domain subspaces. We investigate that partial pre-normality is different from the other weaker kinds of pre-normality. Some results, properties, examples, characterizations and preservation theorems of partial pre-normality were presented.

References

[1] Kuratowski, C. (1958) Topology I, 4th ed. in France, Hafner, New York.

[2] Zaitsev V. (1968) On certain classes of topological spaces and their bicompactifications. Doklady Akademii Nauk SSSR **178:** 778–779.

[3] Dugundji, J. (1992) Topology, Allyn and Bacon, Inc., 470 Atlantic Avenue.

[4] Engelking, R. (1989) General Topology, vol. **6**. Berlin: Heldermann (Sigma series in pure mathematics), Poland.

[5] Patty, C. (1993) Foundation of topology, PWS-KENT Publishing Company, Boston.

[6] Mashhour A. S., El-Monsef M. E. A. and Hasanein I. A. (1984) On pretopological spaces. Bulletin Mathématique de la Société des Scinces Mathématiques de la République Socialiste de Roumanie **28** (76): 39–45

[7] Crossley S. G. and Hildebrand S. K. (1970) Semiclosure. Texas Journal of Science **22**: 99–112

[8] Navalagi G. B. (2000) p-normal, almost p-normal and mildly p-normal spaces. Topology Atlas Preprint ♯ 427

[9] Paul and Bhattacharyya (1995) on p-normal spaces. Soochow Journal of Mathematics **21** (3): 273–289

[10] Alshammari I., Kalantan L. and Thabit S. A. (2019) Partial normality. Journal of Mathematical Analysis **10:** 1–8

[11] Thabit S. A. S.. and Kamaruhaili H. (2012) πp-normal topological spaces. Int. Journal of Math. Analysis **6** (21): 1023–1033.

[12] Mashhour A. S., El-Monsef M .E .A. and El-Deeb S. N. (1982) On precontinuous and weak precontinuous mappings. Proceedings of the Mathematical and Physical Society of Egypt **53:** 47–53.

[13] Bourbaki N. (1951) Topologie general, Paris: Actualites Sci. Ind., nos. Hermann pp. 858–1142.

[14] Park J. H. (2003) Almost p-normal, mildly p-normal spaces and some functions. Chaos, Solitions and Fractals **18:** 267–274.

[15] Thabit, S. A. S. (2013) π-Normality in topological spaces and its generalization. Ph.D Thesis, School of Mathematical Sciences, Universiti Sains Malaysia, USM, Malaysia.

[16] Steen, A. L. and Seebach , J. A. (1995) Counterexamples in Topology., Dover Publications, INC., New York.

[17] Lal S. and Rahman M. S. (1990) A note of quasi-normal spaces. Indian Journal of Mathematics **32** (1): 87–94.

[18] Thabit S. A., Alshammari I. and Alqurashi W. (2021) Epi-quasi normality. Open Mathematics (De Gruyter Open Access), **19**: 1755-1770.

[19] Thabit S. A. S. and Kamaruhaili H. (2011) π-closed sets and almost normality of the niemytzki plane topology. J. Math. Sci. Adv. Appl. **8** (2): 73–85

[20] Ganster M., Jafari S. and Navalagi G.B. (2002) On semi-g-regular and semi-g-normal spaces. Demonstratio Mathematicae **35** (2): 415–421

[21] Levine N. (1970) Generalized closed sets in topology. Rendiconti del Circolo Matematico di Palermo **19:** 89–96.

[22] Sundaram P. and John M. S. (2000) on w-closed sets in topology. Acta Ciencia Indica **4:** 389–392.

[23] Dontchev J. and Noiri T. (2000) Quasi- normal spaces and πg-closed sets. Acta Mathematica Hungarica **89** (3): 211–219.

[24] Maki H., Umbehara J. and Noiri T. (1996) Every topological space is pre-$t_{\frac{1}{2}}$. Memoirs of the Faculty of Science Kochi University Series A (Mathematics) **17**: 33–42

[25] Veerakumar M .K. R. S. (2002) g^*-preclosed sets. Acta Ciencia Indica **XXVIIIM** (1): 51–60.

[26] Sarsak M. S. and Rajesh N. (2010) π-generalized semi-preclosed sets. International Mathematical Forum **5** (12): 573–578.

[27] Janković D. S. (1985) A note on mappings of extremally disconnected spaces. Acta Mathematica Hungarica **46** (1-2): 83–92.

[28] Aslim A., Guler A. G. and Noiri T. (2006) On πgs-closed sets in topological spaces. Acta Mathematica Hungarica, P.T.1 **112** (4): 275–283.

[29] El-Deeb S. N., Hasanein I. A., Mashhour A. S. and Noiri T. (1983) On p-regular spaces. Bull. Math. Soc. Sci. Math. R.S.R. **27(75)** (4): 311–315.

TUJNAS
ISSN-Print: 2073-0764
ISSN-Online: 2959-4340

Thamar University Journal of Natural & Applied Sciences (TUJNAS)

Journal website:
www.tu.edu.ye/journals/index.php/TUJNAS/index

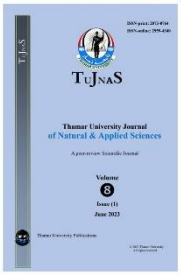

ORIGINAL ARTICLE

Patient's Satisfaction in Radiology Department in Yemen

Abdulwahab M. Y. Al-Mutahar*

Affliations:
Faculty of Medicine and Health Sciences, Thamar University, Dhamar 87246, Yemen

Faculty of Commercialand Economic, Sana'a University, Sana'a, Yemen

Corresponding Author:
Abdulwahab M. Y. Al-Mutahar,
Email: almutahar2000@hotmail.com

Received: Mar 12, 2023,

Accepted Date: May 16, 2023,

Online Date: Jun 12, 2023

Published: Jun 13, 2023

DOI:
https://doi.org/10.59167/tujnas.v8i1.1486

Abstract

Patient satisfaction is one of the most important indicator of quality of care. Patient satisfaction surveys may provide the means for patient to express concerns about the services received, and to express their views about new services needed. Aim of this study was to determine some of the factors that may influence patients' satisfaction with health care services, particularly radiological department in a Yemen. The study was a cross –sectional study was conducted among patients (aged 18-80 years), that targeted patients who presented at the radiology department over the period of three months. 450 patients attending radiology department of the SGH were taken for the study purpose. Data was collecting using a 20 items self-completion questionnaire designed in line with the objectives of the study. Data were categorized into groups and analyzed to draw the patient's satisfaction to the health care services. Out of the 450 patients interviewed for the study, 290 (64.4%) were males and 160 (34.6 %) were females. Majority of the patients (37.3 %) belonged to the age group 20-39 yrs., followed by 36.9 % in the age group 40-50 yrs. There were only (20.9 %) patients who were more than 50 yrs. of age.. When enquired regarding behaviour satisfaction conducted by different staff members Receptionist, 49 % Technician 68 % and doctors 86.8 %. Patient satisfied with behaviour, privacy and time given by doctors but problem lies with the coast and availability of some services and dissatisfaction was found to be more regarding cleanliness in the toilets and the politeness of some receptionist, high temperature, bed sheets, noise, suitable seats availability should be some urgent issues needing concern. Time waiting from appointment is also still a problem issue.

Keywords

Radiology; Patient satisfaction; Yemen

1. Introduction

Health care quality is a global issue. The health care industry is undergoing a rapid transformation to meet the ever-increasing needs and demands of its patient population [1]. The primary goal of the tertiary care hospital as a highest level of health care provision is to provide best possible health care to the patients. The modern era where it is the right of every patient to demand best possible care in hospitals, it is the duty of every staff member of the hospital to deliver his optimum efforts to the entire satisfaction of the patient [2]. Patient satisfaction is one of the established yardsticks to measure success of the services being provided in the health facilities. But it is difficult to measure the satisfaction and gauze responsiveness of the health systems as not only the clinical but also the non-clinical outcomes of care do influence patient satisfaction [3]. There are five main factors that determine patients' satisfaction with health services: Reliability of services, responsiveness to customer needs, assurance-guaranteeing comfort to patients, empathy, and tangibles like physical appearance of the departments and quality of the equipment.

For the information provided to patients to be effective, it must be provided in a format that is easily understood by the patient (or accompanying person if the patient is not capable of understanding). The level of information should be appropriate to the hazard presented. Hospital radiology departments are known to produce very varied instructions to patients [4]. We use Satisfaction questionnaires as a tool to evaluate whether the management of the department and the efforts made obtain a good result [5].

2. Aim and Objectives

This study was to determine some of the factors that may influence patients' satisfaction with health care services, particularly radiological services in a Yemen in tertiary hospital likely Saudi-Germany Hospital-Sana'a Yemen.

Radiological services can be defined simply as services which are rendered to a patient visiting the radiology department, which can be either routine services those carried out on a day-to-day basis or some special examinations that are carried out on special cases that require the use of contrast agents. The aim of this study to assess:

1- Quality of care and patients 'satisfaction in the radiology department in.

2- Improved radiological services based on the information gathered to better address the concerns of the patients and ultimately improve their satisfaction with radiological services.

3. Subjects and methods.

A hospital based cross sectional study was carried out in Saudi-Germani hospital Sana'a, which is a bedded tertiary care hospital. The study was conducted from Oct to Dec 2014. The prevalence used for sample size calculation was 80%. The sample size was inflated by 10% to take care of non-response, incomplete responses and refusals. Patients between the ages of 18 and 80 years attending the outpatient department (OPD) and admitted in various specialties of indoor patient departments (IPD) were referred to radiology department included in the study. However, patients advised for or admitted to the intensive care unit /cardiac care unit /emergency with conditions related to psychiatry or maternity and those with severe acute or chronic illness were excluded from the study since these were considered to be exceptional circumstances.

The questionnaire was given to patients to fill it after having been in the radiology department during the period of the study. A total of 450 questionnaires were distributed; The questionnaire was administered by trained individuals after obtaining verbal consent from all subjects. In order to maintain complete confidentiality no names were recorded on the questionnaire. Prior approval of the ethical board was obtained before beginning the survey. Questionnaires were answered by the patients themselves while illiterates were assessed by a patient relationship staff in the hospital who was blinded to the objective of the study and not a member of the radiology department staff. The questionnaire consists of 20 questions distributed as follows:

- The Socio-demographic profile and residency of the patients: it included the 1st three questions (age and gender).
- Questions were asked before doing examination include receptionist dealing with patient for reservation, waiting time from the appointment was requested until the test was performed, facility of choosing time for the appointment according to availability time for the patient and getting information and explanation regarding the examination.
- Questions were asked about the department including easy to find the radiology department on arrival to the hospital and receive services, politeness of staff with you in the department, the time of waiting from the time of the appointment till attendance and if the patient was told about the waiting time.
- Questions were asked about comfort, including availability of free seats, comfort of the seats, temperature and the noise in the waiting room, cleanliness of the department and toilet.

- Questions were asked about professionals including: Doctors and medical staff listening for complains and questions with care, medical and non-medical staff skills and behavior enough good with respect of privacy of patient, giving you information about the test and if there was any different information given from radiology doctors , opportunity to get a help and ask questions about the test, ensure the confidentiality of the information, respect your privacy during the doing test.
- Questions were asked about satisfaction of the service including: the general satisfaction, come back if he needed in future and if the patient will recommend the department of radiology to another patient due to doctors and staff is qualified and cooperative.

3.1 Scoring of the questionnaire

Socio-demographic section in the questionnaire was scored as follows: gender (0=male, 1=female). Patients indicated their level of satisfaction by selecting responses ranging from poor=1, fair=2, good=3, very good=4 and excellent=5. Those who chose poor, and fair were considered dissatisfied while those who selected good, very good and excellent were considered satisfied.

3.2 Analysis of data

The statistical package SPSS10.0 for Windows XP was used to perform the statistical analysis. As the last two questions are the best questions summarizing the objective of the study nominal regression was calculated to measure which variables, best explained the variability in satisfaction with and recommendation of the department. The results obtained for satisfaction.

4. Results

The Socio- demographic profile in table 1 itself shows the importance of the hospital because majority of the respondent were in the age group of 18-80 years, which is economically productive age group for the families belonging to underserved, needy section of the society. The majority of the study samples were female; (160) 34.6 % male; (290) 64.4 %. With the mean group of age 20-39 years old. In the analysis of the association of the socio demographic variables and recommendations of the radiology department to others, there is a statistically significant difference in the gender with the attitude and behavior of the healthcare providers (Table 1 and 2).

Table 1: Socio-demographic profile of the respondents (n=450)

Characteristics / Age	Male No (%)	Female No (%)	Total No (%)
Under 20 years	19 (4.22%)	3 (0.67%)	22 (4.88 %)
20-39 years	99 (22.%)	69 (15.3%)	168 (37.32%)
40-49 years	94 (20.9%)	72 (16%)	166 (36.9 %)
Over 50 years	78 (17.3%)	16 (3.6%)	94 (20.9 %)
	290(64.4%)	160 (35.6%)	450 (100%)
Geographic Distribution			
Urban	185	103	288 (64%)
Rural	126	36	162 (36%)

It was found that questions about the informed waiting time Q, information before examination Q, noise in the department Q, cleanliness of the department Q, waiting time to appointment Q and conflict of information Q were found to have the highest percentage. The variables statistically affecting the general satisfaction were cleanliness of the department, giving options in choosing the appointment, giving information before appointment regarding the examination or the treatment, waiting time from the time of the appointment was requested until the test was performed in radiology, politeness of persons of the department and being informed about waiting time as shown in (Table 3).

Table 2: Patients satisfaction with the attitude and behavior of the healthcare providers (n=450)

ASPECT OF CARE	SATISFIED in %	DISSATISFIED in %
Behavior of the Receptionist	49 %	51 %
Behavior of the Technician	68 %	32 %
Behavior of the Doctors	86.8 %	13.2 %

Table 3: Availability of General basic facilities in the hospital (n=450)

AVAILABILITY OF FACILITIES	ADEQUATE (%)	INADEQUATE (%)
Toilets	60 %	40 %
Noise	57 %	43 %
Cleanliness	65 %	35 %
Location of Department	88 %	12 %
Waiting room /seating availability & comfort	56 %	43 %
Temperature	74 %	26 %

The variables which statistically affected recommendation of the imaging radiology to the others were giving options in choosing the appointment, waiting time from the time of the appointment was requested until the test was performed in the radiology department, clean toilets, giving information before appointment regarding the examination or the treatment, conflict of information, cleanliness and noise in the department as shown in (Table 3). In the analysis of the percentage of dissatisfaction for the overall questionnaire (Table 4).

Table 4: Patient's satisfaction to radiology services.

PATIENT OVERALL RATING					
Care	**Excellent**	**Very good**	**Good**	**Fair**	**Poor**
Doctor-patient	30	22	5.4	28.5	13.9
General facilities availability	26.8	33	11.1	13	6.1
Information & support	43	25	3	13	6.1
Department care	30	27.5	21.8	15	5.7
General satisfaction	35	26	17.5	14.7	6.6

5. Discussion

Satisfaction is a multi-dimensional concept influenced by preconceived thoughts or even previous experiences, which make its measurements and comprehension difficult as an isolated concept. Measurement of satisfaction is part of a concept, which is difficult to quantify and even define. Many authors define it as a subjective concept aimed at relating the grade at which health care responds to the expectations of the patient or community. Satisfaction questionnaires in patients receiving health care are useful tools when evaluating whether the

management of the department and the efforts made obtain a good result [6]. Different studies have found a strong association between the perception of the global quality of a department and the satisfaction of the patients.

In our study, the socio-demographic characteristics of participants showed that most of them were males (64.4 %). This result controversial with Caminals study [4] which reported that 58% of those surveyed were women. The socio-demographic characteristics (gender, geographic distribution and health status) significantly affect the overall impression on the radiology department. Gender only significantly affect the recommendation of the department to the others and this agrees with Andres *et al.* [7], while it was controversial with Perez *et al.,* study [6], who reported that socio-demographic characteristics did not affect the overall impression or recommendation of the department to the others.

The social aspects result like giving information about waiting time, information before examination and conflict information were unsatisfactory to the patients. This explained by low level of education of most the patients and many procedures of imaging radiology includes many steps as some cases of scan required preparation, fasting or dynamic images or IV contrast (need creatine test) prior to the IVP,CT and angiogram test. Reception of the patients on arrival will affect their satisfaction since the successful application of medical knowledge depends on the patients' perception of hospital personnel and the hospital itself, radiodiagnostic services found that adequate explanation and instruction to the patient about the procedure before the examination that is carried out is necessary since it significantly contributes to obtaining a good diagnostic image [8].

In our study, patients were not satisfied with the degree of cleanliness and noise in the department and these results disagree with Okaro *et al.,* study [9], who reported that the waiting areas were recognize as uncomfortable by 83.7% of the study population. In our study, the waiting time from the time of the appointment was requested until the test was perform in imaging radiology or the length of the waiting time greatly affected satisfaction of the patients, and this agrees with many of studies [10] which consider waiting time as an important parameter in affecting the satisfaction of health care user.

Respect for privacy dissatisfaction may be attributed in part to the poor conditions of changing rooms, waiting areas, and design of examination rooms. Patients often feel a sense of intrusion of their privacy, when the examination rooms are not guarded against other staff and patients. Staff attitude and courtesy are among high dissatisfaction levels which may also be partially attributed to a large number of patients who visit this facility, each expecting to leave early and may sometimes lead to altercations between receptionist and patients. Staff were,

however, not justified to be of bad behavior to patients based on this reason. This is in line with the study conducted in Ghana, but this is in contrast with the study conducted in Ethiopia, which shows high satisfaction level in that item [11].

6. Conclusions

This study shows assessing satisfaction of patients is simple, easy and cost-effective way for evaluation of hospital services and has helped finding that patients admitted in SGH Sana'a Hospital were more satisfied with behavior of doctors, but problem lies with the coast and availability of some services and dissatisfaction was found to be more regarding cleanliness in the toilets and the politeness of some receptionist. Bed sheets, noise, suitable seats. High temperature availability should be some urgent issues needing concern. Time waiting from appointment is also still a problem issue.

Patients' satisfaction is greatly affected by many factors which can be improved by the radiology department staff dealing pattern as waiting time, cleanliness of the department and most these factors can be refined by improving the system of booking and registration and training the department staff to simplify the imaging radiology procedure to the patient and prepare them for any unexpected changes in the time schedule.

Certain improvements are also needed in the waiting area by making it informative and comfortable. Hospital administration should ensure that all the equipment's are working properly and well maintained. The fact that some patients expressed dissatisfaction with the services indicates that health care providers need to do more in the drive towards improving service windows in order to improve efficiency, minimize patient waiting times and provide for patient comfort. Periodic patient satisfaction survey should be institutionalized to provide feedback for continuous quality improvement.

References

[1] Qadri, S.S., Pathak, R., Singh, M., Ahluwalia, S., Saini, S., Garg, P. (2012) An assessment of patients satisfaction with services obtained from a tertiary care hospital in rural Haryana, *International Journal of Collaborative Research on Internal Medicine & Public Health* **4(8)**: 1524-1537.

[2] Singh, S., Kaur, P., Rochwani, R. (2013) Patient satisfaction levels in a tertiary care medical college hospital in Punjab, North India, *International Journal of Research and Development of Health* **1(4)**: 172-82.

[3] Hamed, M.A.G., Salem, G.M. (2014) Factors affecting patients' satisfaction in nuclear medicine department in Egypt, *The Egyptian Journal of Radiology and Nuclear Medicine* **45(1)**: 219-224.

[4] Caminal, J. (2001) La medida de la satisfacción: un instrumento de participación de la población en la mejora de la calidad de los servicios sanitarios, *Revista de Calidad Asistencial* **16(4)**: 276-279.

[5] Vicente, A.G., Castrejón, A.S., Delgado, C.M., García, V.P., Solís, S.R., Romera, M.C., Marina, S.R. (2007) Patient satisfaction as quality indicator in a Nuclear Medicine Department, *Revista española de medicina nuclear (English Edition)* **26(3)**: 146-152.

[6] Reyes-Pérez, M., Rodrigo-Rincón, M., Martínez-Lozano, M., Goñi-Gironés, E., Camarero-Salazar, A., Serra-Arbeloa, P., Estébanez-Estébanez, C. (2012) Assessment of the patient satisfaction with a nuclear medicine service, *Revista Española de Medicina Nuclear e Imagen Molecular (English Edition)* **31(4)**: 192-201.

[7] Andrés, M., García-Castrillo, L., Rubini, S., Juárez, R., Skaf, E., Fernández, M., Llorens, P., Álvarez, A., Vegas, F., Epelde, F. (2007) Evaluación del efecto de la información en la satisfacción de los pacientes atendidos en los servicios de urgencias hospitalarios, *Revista de Calidad Asistencial* **22(4)**: 161-167.

[8] Young, G.J., Meterko, M., Desai, K.R. (2000) Patient satisfaction with hospital care: effects of demographic and institutional characteristics, *Medical care* **38(3)**: 325-334.

[9] Okaro, A., Ohagwu, C., Njoku, J. (2010) Evaluation of patient care in radio-diagnostic departments in Enugu, Nigeria, *European Journal of Scientific Research* **41(2)**: 309-13.

[10] Sanitario, B. (2010) Instituto de Información Sanitaria, Ministerio de Sanidad, Política Social e Igualdad, Madrid, pp. 45.

[11] Wahed, W., Mabrook, S., Abdel Wahed, W. (2017) Assessment of patient satisfaction at radiological department of Fayoum University Hospitals, *International Journal of Medicine in Developing Countries* **1(3)**: 126-131.

TUJNAS
ISSN-Print: 2073-0764
ISSN-Online: 2959-4340

Thamar University Journal of
Natural & Applied Sciences
(TUJNAS)

Journal website:
www.tu.edu.ye/journals/index.php/TUJNAS/index

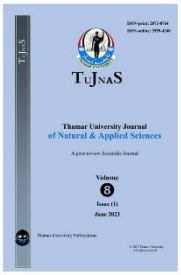

ORIGINAL ARTICLE

Hybrid Filter-Genetic Feature Selection Method For Arabic Sentiment Analysis

Muneer A.S. Hazaa[1]* and Saleh Ahmed Ali Hussein Salah[2]*

Affliations:
[1] Faculty of Computer And Information Systems ,Thamar University, Dhamar 87246, Yemen

[2] Yemen Academy For Graduate Studies Sana'a, Yemen

Corresponding Authors:
Muneer A.S. Hazaa, email: muneer_hazaa@yahoo.com and Saleh A. A. H. Salah, email: salehhazzeb@gmail.com

Received: Mar 12, 2023,

Accepted Date: May 16, 2023,

Online Date: Jun 12, 2023

Published: Jun 13, 2023

DOI:
https://doi.org/10.59167/tujnas.v8i1.1487

Abstract

The dramatic increase in user comments describing their feelings about products, services, and events brings sentiment analysis to the forefront as a way to monitor public opinion about products and events. Feature selection is an important subtask of sentiment analysis, which aims to improve the performance of learning algorithms and reduce the dimensionality of a problem. Feature selection is an important subtask of sentiment analysis, as it can improve the performance of learning algorithms while reducing the dimensionality of a problem. Moreover, the high-dimensional feature spaces caused by the morphological richness of Arabic motivate further research in this area. In this paper, a hybrid filter-based and genetic feature selection algorithm is proposed using four machine learning algorithms, namely decision tree, Naive-Bayes, K-NN and meta-ensemble methods. The performance of the proposed algorithm is compared with the performance of baseline models. A wide range of experiments are conducted on two standard Arabic datasets. The experimental results clearly show that the improved methods outperform the other baseline models for Arabic sentiment analysis. The results show that the improved models outperform traditional approaches in terms of classification accuracy, with a 5% increase in the macro average of F1.

Keywords

Machin Learning; Sentiment Analysis; Opinion Mining; Feature Selection; Arabic

1. Introduction

Given the large amount of online opinions and reviews provided by social media users about strategies, services, and products, understanding the extremely important information in social media content is of great value to many interested groups such as customers, business owners, and stakeholders. People use social media for a variety of purposes, including expressing their views on products and policies, leading various parties such as customers, businesses, and governments to begin analyzing those opinions. In fact, customer opinions and ratings play an important role in decision-making processes. In particular, decision makers take into account the experiences of their peers when making decisions, which consume valuable resources such as time and/or money. Identifying and analyzing customer opinions in an efficient and correct way to understand both current and potential customer needs has become a critical challenge for market-oriented product design.

Sentiment analysis is about identifying and analyzing explicit or implicit feelings and emotions expressed in posts on social media [1, 2]. Sentiment analysis is an important research area in the field of natural language processing (NLP). Sentiment analysis is a special type of text classification in which the general sentiment expressed in a review is classified into either positive or negative classes. As with any classification task, there are various methods and approaches for sentiment classification and opinion mining. Most of these methods and approaches can be divided into two main methods: supervised [3-7] and unsupervised learning approaches [1, 8, 9]. In supervised machine learning, sentiment corpora are used to train classifiers. Unsupervised approaches, also known as lexicon-based approaches, estimate the sentiment polarity of a text based on the subjective alignment of words or phrases [1, 8].

As part of sentiment analysis, feature selection is an important task that can significantly improve the performance of sentiment analysis [3, 5, 10, 11]. Feature selection is an important step to shorten the processing time and improve the analysis accuracy by reducing the feature sizes. In general, feature selection methods can be divided into two types: statistical methods and meta-heuristic methods. Statistical methods usually consist of two steps, feature evaluation and selection of the best subset. Meta-heuristics based feature selection methods are divided into four steps: Generation of initial subsets, evaluation of subsets, generation of next iteration, stopping criteria, and verification of results. Statistical methods are time-saving and provide faster results, while meta-heuristic feature selection is power-efficient as it can significantly improve accuracy. To combine the strengths of these approaches, a filter-based guided meta-heuristic feature-based method is introduced in this paper to improve the time and performance efficiency of the meta-heuristic method. The key ideas are based on reducing the search space

for meta-heuristic feature selection. In the new paper, we propose two layers of feature selection methods that combine a genetic algorithm with traditional feature selection methods. In addition, this paper evaluates four machine learning algorithms - decision tree, Naive-Bayes, K-NN, and meta-ensemble - with the proposed feature selection method.

The remainder of this paper is organized as follows. Section 2 presents related work, while Section 3 describes the methodology as well as the classification modules and feature selection methods. In Section 4, we present the experimental setup. Section 5 discusses the experimental results. Finally, we conclude our work and discuss future research directions in section 6.

2. Related Work

This section provides a review of techniques proposed for analysis sentiment and Arabic subjectivity including feature selection and extraction and sentiment analysis. Abbasi, *et al.* [12] proposed a system for sentiment analysis task in a multi-language web forum at the document level. The system depends on an Entropy-Weighted Genetic Algorithm (EWGA) to choose the best features, and the Support Vectore Machine (SVM) with the linear kernel for the sentiment classification. Their method tries to find an over- lap between language-independent features, including syntactic and stylistic features and This research applied developed the Entropy Weighted Genetic Algorithm (EWGA) for efficient feature selection in order to improve accuracy and identify key features for each sentiment class. This research study applied developed the Entropy Weighted Genetic Algorithm (EWGA) for efficient feature selection in order to improve accuracy and identify key features for each sentiment class.

Another group of researchers Rushdi-Saleh, *et al.*, [13] focused on investigating two machine learning (ML) classifiers, Naive Bayes and Support Vector Machine(SVM), with two different weighting schemes (term frequency and term frequency-inverse document frequency) and three n-gram models. The effect of using the stem of the Arabic work has also been studied with different n-gramme models in Arabic and English corpora. The Arabic corpora consist of 500 reviews (250 positive and 250 negative). The results show that SVM with the tri-gramme model and without stemming achieved an F-value of 90% in the Arabic corpus and 86.9% in the English corpus.

Al-Moslmi *et al*., [5] and Omar *et al*., [3, 4] present detailed study concerning the effect of the feature selection technique on Arabic and Malay sentiment analysis. They present an empirical comparison of seven feature selection methods (Information Gain, Principal Components Analysis, ReliefF, Gini Index, Uncertainty, Chi-squared, and Support Vector

Machines), and three classifiers (SVM, Naïve Bayes, and K-nearest neighbor).

In [14] present two different hierarchical classifiers and compared their accuracy with the flat classifiers using three different classifiers namely Support Vector Machines (SVM), Naïve Bayes, (NB), and K-nearest neighbor (KNN) . The results showed that, in general, hierarchical classifiers gave significant improvements over flat classifiers.

3. Methodology

In this work, we create a unified framework that includes all the tasks required for sentiment analysis. This modular method allows us to study different approaches to Arabic sentiment analysis, focusing on feature selection. The proposed framework consists of different phases ranging from preprocessing, data representation, feature selection, and sentiment analysis, as shown in Figure 1. The main goal of this work is to develop two layers of feature selection methods that combine a genetic algorithm with traditional feature selection methods. In addition, these models use an ensemble machine learning method where a meta-classifier is used to combine the results of the basic machine learning method.

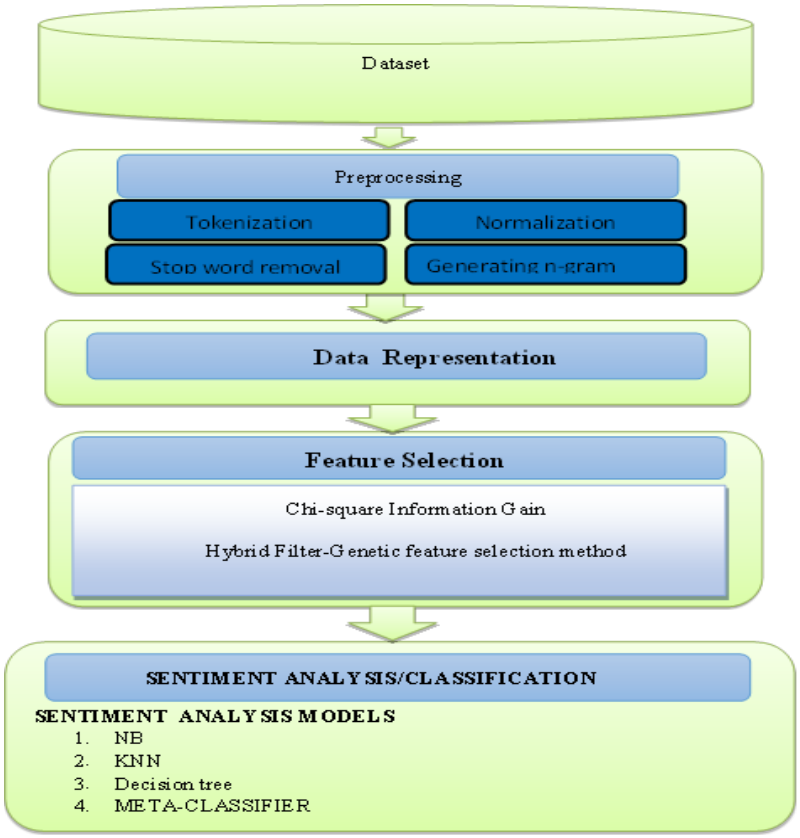

Figure 1. The framework of the implementation of the Arabic sentiment analysis/classification models.

A. Pre-Processing

Reviews usually include noisy data, recurring characters, spelling errors, and Html codes. Therefore, it is crucial to pre-process the data before analysis them using machine learning approaches. In the pre-processing phase, several NLP techniques were applied. The pre-processing here consists of four steps, namely: 1) tokenization; 2) normalization; and 3) stop word removal 4) Generating N-Gram Elements. In normalization, the raw data collected from social media is not 100% pure, so it contains a lot of noise. In this step, first, any non-Arabic words or characters that may belong to HTML, links, or the programming language code have been removed from the text. In tokenization, each review is spilt into sentences and words. It converted to a bag of words representation. Tokenization depends on the use of punctuation marks and white spaces in delimiting word boundaries (or main tokens). All texts including reviews contain many stop words such as pronouns, prepositions, and conjunctions. These words are removed as they do not provide worthless information about class or cluster of any text. in generating n-gram elements, each review is represented as a bag of both bigrams and unigrams which are useful to train a sentiment classifier (Bollegala et al. 2013). Based on that, a review was modeled as a bag of words to obtain unigrams and bigrams from each sentence.

B. Data Reprsentation Phase

Text representation focuses on how to convert pre-processed text to build the feature vectors and how to assign weights to the elements of the vector. In this paper, dataset is represented as a matrix (table) in which the columns represent the n-grams unigram and bigram in the reviews and the values represent their frequencies in a review. Each row is used to represent a review. Therefore, each review R_i is represented as$R_i = (a_{i1}a_{i2}, \ldots\ldots, a_{im})$, where a_{ij} is the frequency of n-gram $g_j$in the review R_i . This value can be calculated in various ways.

C. Feature Selection Phase

The size of features generated after the preprocessing phase in a text mining task is relatively huge (i.e., the curse of dimensionality). The process of selecting discriminating independent features is critical to any text mining that hopes to be effective in classification. Most of these features are not informative or cannot provide high discrimination. In general, several thousands of features are obtained, only an extremely small percentage of these features convey valuable information towards sentiment analysis objective. Subsequently, we typically need an algorithm that compresses the obtained feature vector and reduces its dimension. This work proposes two layers feature selection that uses filter-based methods (information gain and chi-squared) and genetic algorithm as feature reduction techniques.

Layer 1: Scoring Features Using Filtering Based Methods:

The first layer uses filter-based feature selection methods to score individual features according to their discriminative ability, i.e., their capability of separating the classes. To this end, A feature with a high-ranking value indicates higher discrimination of this feature compared to other categories and means that the feature contains information potentially useful for classification. Based on the ranking value they obtain; features are then returned in an ordered list where they appear in descending order of relevance. A subset of top n ranked features is selected. This work uses the following most widely used feature selection which proves to be efficient for sentiment analysis:

Information Gain.

The information gain (IG) method is used in the ranking and selecting the most relevant features. Information gain (IG) measures the relevance of a feature to a class. Information gain (IG) is a very popular method in feature selection (FS). It is used as a measure for feature goodness in the area of machine learning (ML). IG calculates the information amount that is present in or absent from a feature. The value obtained in the calculation of IG for each attribute is useful in determining the correct classification of any class.

$$IG(t) = -\sum_{i=1}^{|c|} p(c_i) \log p(c_i) + p(t) \sum_{i=1}^{|c|} p(c_i|t) \log p(c_i|t) + p(\bar{t}) \sum_{i=1}^{|c|} p(c_i|\bar{t}) \log p(c_i|\bar{t}) \quad (1)$$

Where $p(c_i)$denotes the probability that class $c_i$occurs; $p(t)$ denotes the probability that term t occurs, and $p(\bar{t})$ denotes the probability that word $\bar{t}$ does not occur.

Chi-Squared Statistic (χ^2): χ^2 is one of the most widely used filter-based feature selection algorithms. The $\chi 2$ value for each feature t in class c is calculated by the following equation:

$$\chi^2(c,t) = \frac{N \times (\text{AD-BC})}{(A+C)(B+C)(A+B)(C+D)} \quad (2)$$

$$\chi_{\max}{}^2(t) = \max_i (\chi^2(t, c_i)) \quad (3)$$

Where N is the total count of training reviews while A is the number of Arabic reviews have class c and contains features t, and B is the number of Arabic reviews that do not belong to class c but contains feature t. Meanwhile, C is the number of Arabic reviews that do not belong to class c and do not contain feature t. D is the number of Arabic reviews that do not belong to class c and do not contain term t.

Layer 2: Selecting Final Feature Subset

A GA is a heuristic search algorithm that mimics the natural evolution process of man. Given the top n selected features from the filter-based method, the proposed hybrid meta-heuristic of GAs is applied on these selected features to determine the minimal subset of features, for which the different classes are best distinguished during sentiment analysis. GA has five important steps which include Generation of Initial Population, fitness evaluation, selection mechanisms, genetic operators and criteria to stop the GA. The following describes the main steps of the GA algorithm and how it combined with the Filter based method.

a). Population initialization (selects n chromosomes randomly): The initial population here is an n chromosome, each Chromosome has Length m which consists of a vector of chromosomes (genotype), which is a Boolean vector indicating if a feature should be included or not. The Population Size is the number of chromosomes (individuals) in the population, while Chromosome Length (Genome Length) is the number of bits (genes) in each chromosome. The GA is iteratively performed over several generations and reproduction is performed to obtain individuals that are a best fit for a certain environment.

b). Fitness computation: Fitness is the key component of the genetic algorithm and is used to calculate how well a chromosome is suited to the environment and only chromosomes with high fitness will survive over time. First, the algorithm evaluates each chromosome Cu. The fitness of each chromosome in this work is evaluated using MI-based fitness function using Equation:

$$\mathrm{MI}\ (\mathrm{f}, \mathrm{c}) = \log \frac{\mathrm{p}(\mathrm{f} \wedge \mathrm{c})}{\mathrm{p}(\mathrm{f}) \times \mathrm{p}\ (\mathrm{c})} \qquad (4)$$

c). Selection operation: The algorithm then sorts the n chromosomes in the descending order of their fitness values. The algorithm then chooses the n/2 number of best chromosomes from the initial population of n chromosomes using the fitness function.

c) Crossover operation: The algorithm sorts the |n/2| chromosomes in descending order according to their fitness values. All chromosomes participate in the crossover operation pair by pair since for a crossover operation we need a pair of chromosomes. Then the algorithm applies the twin removal operation on the new population made of the offspring chromosomes.

d) Mutation operation: The basic idea of the mutation operation is to randomly change some of the chromosomes to explore different solutions. While adding random changes

to the chromosomes, the algorithm uses a probabilistic approach where a chromosome with a low fitness has a high probability of getting a random change, and vice versa.

e) Stopping Criteria: After a certain number of iteration where steps a) to d) are repeated, the best chromosome in the last iteration is selected. The best chromosome consists of several selected features

D. Classification Phase

In this section, we have briefly described the classification approaches used in this work. These approaches have been used to classify the comments or reviews written in Arabic as positive and negative classes. The following subsection briefly describes the classification approaches used in this paper.

1) Decision Tree

A Decision tree is a supervised hierarchical machine learning model for inducing a decision tree from training data. The decision tree a predictive model which is a mapping from features of an item to classification about its target value. In the decision tree structures, leaves represent classifications, non-leaf nodes are features, and branches represent conjunctions of features that lead to the classifications The classes are represented by the leafs. In this work, the decision tree classifier J48 is used. J48 is a decision tree classifier in which an attribute is selected based on information gain from the training data to build each node of the tree. The selected attributes effectively split a set of training data into subsets enriched in one class or the other. It is mostly used because of its simplicity in explanation and interpretation. However, to find the best ordering features, all available features must be ranked. Therefore, entropy-based measure such as information gain based on the input training set S and a single feature F, with following equation:

$$\text{InformationGain}(S, F) = \text{Entropy}(S) - \text{Average entropy}(S, F). \quad (5)$$

The average entropy is defined by the following formula,

$$\text{Average entropy}(S, F) = \sum_i \frac{|s_i|}{s} \text{Entropy}(S_i) \quad (6)$$

2) Naive Bayes (NB) Classifier

The Naive Bayes (NB) algorithm is a widely used algorithm for sentiment analysis. Given a feature vector table, the algorithm computes the posterior probability that the document belongs to different classes and assigns it to the class with the highest posterior probability. The major advantage of NB sentinement analysis algorithms is that they are easy to implement, often they have superior performance.

3) K-Nearest Neighbour(K- NN)

The K-nearest neighbor (KNN) is a typical example-based classifier. Given a test document d, the system finds the K-nearest neighbors among training documents. The similarity score of each nearest neighbor's document to the test document is used as the weight of the classes in the neighbor's document. The weighted sum in KNN categorization can be written as in Equation 3.10:

$$\text{score}(d, t_i) = \sum_{d_j=KNN(d)} sim(d, d_j)\ \delta(d_j, c_i) \quad (7)$$

Where KNN *(d)* indicates the set of K- nearest neighbours of document *d.* If d_jBelongs toc_i, $\delta(d_j, c_i)$ equals 1, or other-wise 0. For test document$d$, it should belong to the class that has the highest resulting weighted sum.

4) Stacking Classifier Combination : Meta-Classification

The stacking classifier combination is an ensemble machine learning technique to combine multiple classification models via a meta-classifier. The base classification models are trained based on the complete or percentage of the training set; then, the meta-classifier is trained based on the outputs of the base classification models in the ensemble. The output for all base classifiers is considered as a new feature for meta-learning. The classification model used for this purpose is Naïve Bayes.The stacking combination involves two phases. The first phase involves the construction of a set of base-level classifiers (individual classifiers). The second phase involves the combination of the output of the base-level classifiers into a meta-level classifier. When a meta-classifier is used to combine the classifiers, the outputs of all the labels of the classes of the participating classifiers will be used as features for meta-learning.

hybrid approach

A hybrid approach that was crafted to improve the performance measures of sentiment analysis for the Arabic Language. This study focused on tweets sentiment classification for Egyptian dialect. Arabic is one of the widely used languages on the web [12]. Many researchers have worked on Arabic language sentiment analysis on different data sets with different tools and algorithms [13].

Following steps were carried out by the researcher for the implementation of the hybrid technique:

- Step 1: The features to be used by the machine learning approach are identified and separated.
- Step 2: The annotated corpus to be used for training and validation of the best classifier at different corpus sizes is built by the system.
- Step 3: Sentiment lexicon of different sizes is built using the annotated corpus
- Step 4: Theses different approaches are combined and tested for better and optimized results
- Step 5: Straight forward and simple method is crafted to detect negations in the hybrid approach

The results obtained by this study using hybrid approach showed better performance than other sentence-level classification systems.

4. Experimental Setting

Several experiments will be carried out to assess the proposed Arabic sentiment analysis models. First, many of experiments were carried out to measure the performance of the traditional machine learning models namely decision tree (DT), K-nearest neighbor classifier (KNN), Naive Bayes (NB) and meta-classification ensemble machine learning method with traditional feature selection methods namely information gain and chi-squared for Arabic opinion and sentiment analysis. Next, several experiments were performed to evaluate the proposed filter-based Directed Genetic optimized feature selection method with all classification models. All experiments are carried out using two datasets (1) opinion corpus for Arabic (OCA) [13]. The corpus comprises 500 reviews retrieved from a web page and blogs. From the 500 reviews in the OCA, 250 are listed as positive opinion reviews while 250 are negative opinion reviews. (2) Multi-domain Arabic Sentiment Corpus (MASC) [1]. The total number of reviews in the corpus is 8,860 reviews. The total positive reviews amount to 5408; while the total negative documents amount to 3453. The standard classification measurement precision, recall, and F-measure are used to assess the proposed model. Finally, all the experiments are performed on both corpora which are divided into 90% for training the proposed model, while 10% used for testing.

5. Results and Discussion

First, several experiments are conducted to evaluates the four baseline Arabic sentiment analysis models (decision tree (DT), K-nearest neighbor classifier (KNN), Naive Bayes (NB) and meta-classification ensemble method) along with Information gain and Chi-square. Figure 2, the performance (F-measure) the best results obtained by baseline Arabic sentiment analysis

models with Information Gain (IG) and Chi-square (CHI) feature selection method on OCA and MASC. It can be observed that the enhanced meta-classification ensemble model (e-MT) outperforms other baseline classifiers with two feature selection methods. Furthermore, the meta-classification ensemble model achieved the best performance results with all datasets. The meta-classifier combines the strength of its individuals (base-classifiers). It expected when several individual classifiers agree on classifying most of the cases and only disagree with small cases (when one of them becomes wrong), then combining these classifiers always achieves higher results. Besides, combining the decision of several single classifiers which achieve a high result, better than individual classifier (base-classifier).

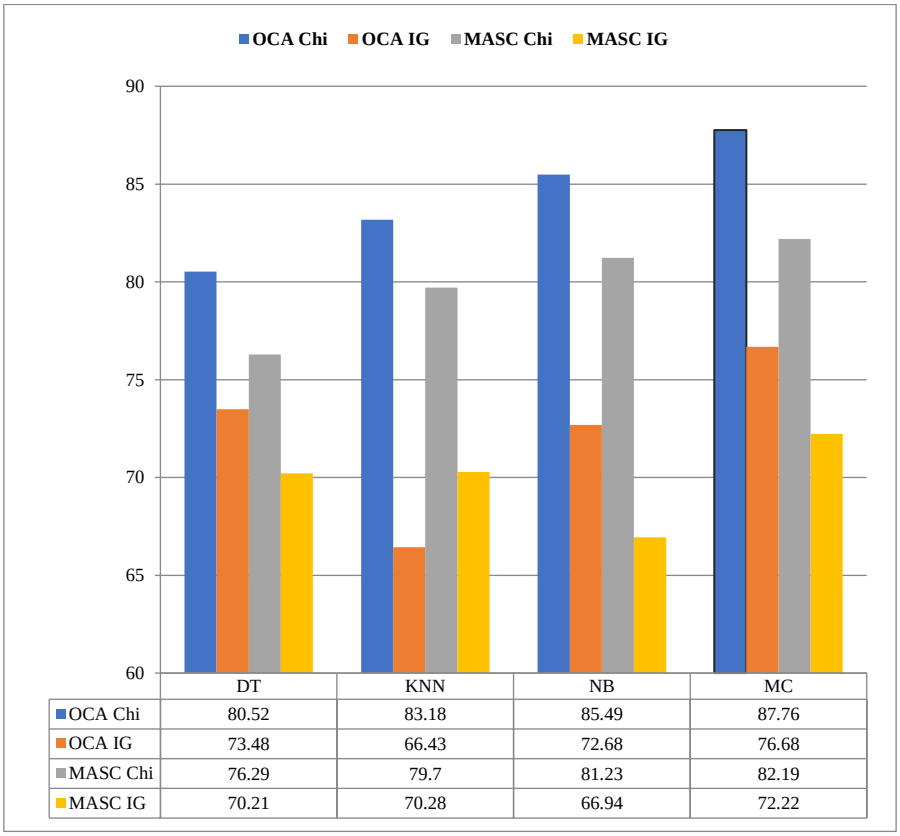

	DT	KNN	NB	MC
OCA Chi	80.52	83.18	85.49	87.76
OCA IG	73.48	66.43	72.68	76.68
MASC Chi	76.29	79.7	81.23	82.19
MASC IG	70.21	70.28	66.94	72.22

Figure 2. Performance (F-measure) the best results obtained by baseline Arabic sentiment analysis models with IG and CHI on OCA and MASC.

Second, several experiments are conducted to study the effect of the proposed two-layer filter-based Genetic (TF_GenFS) feature selection method on the four Arabic sentiment analysis models. Table 1 shows the results of four enhanced classification models on both opinion corpuses for Arabic (OCA) and Multi-domain Arabic Sentiment Corpus (MASC). The results obtained show that the results of all classification models are significantly improved with the proposed two-layer filter-based Genetic (TF_GenFS) feature selection method. It can

also be observed that the enhanced meta-classification ensemble model (MT) with the proposed TF_GenFS feature selection outperforms other classification models. These findings reveal that the classifier combination method with the proposed TF_GenFS feature selection method is the most suitable technique for Arabic sentiment analysis.

Table 1: Performance (F-measure) of enhanced Arabic sentiment analysis models on OCA and MASC.

	OCA	**MASC**
DT+TF-GenFS	84.96	80.26
KNN+TF-GenFS	89.15	83.61
NB+TF-GenFS	90.43	85.49
MC+TF-GenFS	93.74	87.01

6. Conclusions

This paper empirically evaluates four machine learning methods namely decision tree (DT), K-nearest neighbor classifier (KNN), Naive Bayes (NB) and meta-classification ensemble method with information gain and chi-squared traditional feature selection methods for Arabic opinion and sentiment analysis task. In addition, this paper introduces enhanced Arabic opinion and sentiment analysis models based on a two-layer filter based Genetic feature selection method. This paper demonstrates that using the two-layer filter based Genetic feature selection method improve the performance of all four machine learning methods for Arabic sentiment classification. Experimental results demonstrate these findings reveal that the classifier combination method with the proposed feature selection method is the most suitable technique for Arabic sentiment analysis.

References

[1] Al-Moslmi, T., Albared, M., Al-Shabi, A., Omar, N., Abdullah, S. (2018) Arabic senti-lexicon: Constructing publicly available language resources for Arabic sentiment analysis, *Journal of information science* **44**: 345-362.

[2] Yue, L., Chen, W., Li, X., Zuo, W., Yin, M. (2019) A survey of sentiment analysis in social media, *Knowledge and Information Systems* 1-47.

[3] Omar, N., Albared, M., Al-Moslmi, T., Al-Shabi, A. (2014) A comparative study of feature selection and machine learning algorithms for Arabic sentiment classification, Asia information retrieval symposium, Springer, pp. 429-443.

[4] Omar, N., Albared, M., Al-Shabi, A.Q., Al-Moslmi, T. (2013) Ensemble of classification algorithms for subjectivity and sentiment analysis of Arabic customers' reviews, *International Journal of Advancements in Computing Technology* **5**: 77.

[5] Al-Moslmi, T., Gaber, S., Al-Shabi, A., Albared, M., Omar, N. (2015) Feature selection methods effects on machine learning approaches in malay sentiment analysis, Proc. 1st ICRIL-Int. Conf. Inno. Sci. Technol.(IICIST), pp. 1-2.

[6] Tuhin, R.A., Paul, B.K., Nawrine, F., Akter, M., Das, A.K. (2019) An Automated System of Sentiment Analysis from Bangla Text using Supervised Learning Techniques, 2019 IEEE 4th International Conference on Computer and Communication Systems (ICCCS), IEEE, pp. 360-364.

[7] Silva, N.F.F.D., Coletta, L.F., Hruschka, E.R. (2016) A survey and comparative study of tweet sentiment analysis via semi-supervised learning, *ACM Computing Surveys (CSUR)* **49**: 1-26.

[8] Khoo, C.S., Johnkhan, S.B. (2018) Lexicon-based sentiment analysis: Comparative evaluation of six sentiment lexicons, *Journal of Information Science* **44**: 491-511.

[9] Al-Saffar, A., Awang, S., Tao, H., Omar, N., Al-Saiagh, W., Al-bared, M. (2018) Malay sentiment analysis based on combined classification approaches and Senti-lexicon algorithm, *PloS one* **13**: e0194852.

[10] Madasu, A., Elango, S. (2020) Efficient feature selection techniques for sentiment analysis, *Multimedia Tools and Applications* **79**: 6313-6335.

[11] Gokalp, O., Tasci, E., Ugur, A. (2020) A novel wrapper feature selection algorithm based on iterated greedy metaheuristic for sentiment classification, *Expert Systems with Applications* **146**: 113176.

[12] Abbasi, A., Chen, H., Salem, A. (2008) Sentiment analysis in multiple languages: Feature selection for opinion classification in web forums, *ACM Transactions on Information Systems (TOIS)* **26**: 1-34.

[13] Rushdi-Saleh, M., Martín-Valdivia, M.T., Ureña-López, L.A., Perea-Ortega, J.M. (2011) OCA: Opinion corpus for Arabic, *Journal of the American Society for Information Science and Technology* **62**: 2045-2054.

[14] Al-Ayyoub, M., Nuseir, A., Kanaan, G., Al-Shalabi, R. (2016) Hierar-chical classifiers for multi-way sentiment analysis of arabic reviews, *International Journal of Advanced Computer Science and Applications (IJACSA)* **7**: 531-539.

TUJNAS
ISSN-Print: 2073-0764
ISSN-Online: 2959-4340

Thamar University Journal of
Natural & Applied Sciences
(TUJNAS)

Journal website:
www.tu.edu.ye/journals/index.php/TUJNAS/index

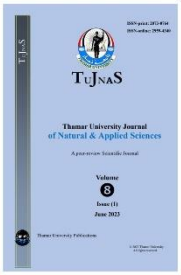

ORIGINAL ARTICLE

Photo-Electrical Tandem of Modulated Polyvinyl Alcohol Based Plasticized Solid Polymer Electrolyte Nanocomposite Films: Effect of Propylene Carbonate Contents

Murad Q. A. Al-Gunaid[1]*, Waled Abdo Ahmed[1], Mohammed. A. dhif-Allah[2], Fares H. Al-Ostoot[3]

Affliations:
[1]Department of Chemistry, Faculty of Education, Thamar University, Dhamar 87246, Yemen

[2]Department of Agriculture, Faculty of Agriculture, Thamar University, Dhamar 87246, Yemen

[3]Department of Biochemistry, Faculty of Education and Science, Al-Baydha University, Al-Baydha, Yemen.

Corresponding Author:
Murad Q. A. Al-Gunaid, emails: morad.jounid11@gmail.com, or MuradAl-Gunaid11@tu.edu.ye

Received: Mar 21, 2023,

Revised Date: Apr 20, 2023,

Accepted Date: May 8, 2023,

Online Date: Jun 12, 2023

Published: Jun 13, 2023

DOI:
https://doi.org/10.59167/tujnas.v8i1.1490

Abstract

Plasticized solid polymeric electrolyte nanocomposites based on polyvinyl alcohol (PVA) incorporating Cs_2CuO_2 nanoparticles (NPs), electrolyte salt ($LiClO_4$) and plasticizer (PC) were prepared via solution casting technique. The dynamic light-scattering histogram revealed that the prepared Cs_2CuO_2 NPs have a size in the range of 80-120 nm. The interaction between different components in PVA/Cs_2CuO_2/$LiClO_4$-PC films (plasticized PVA-SPEs) were probed by FTIR, while the surface and structure were evaluated by SEM and XRD, which indicate to amorphous nature of plasticized PVA-SPEs. The thermal behavior of films was measured via TGA, where a partial decrease in the thermal stability of films was noticed with an increase of PC content in the PVA-SPEs. The highest conductivity achieved is $9.56X10^{-5}$ S/cm for PVA-SPEs containing 8wt% PC at 298K. The plasticized PVA-SPEs exhibited higher specific capacitance by two folds and photovoltaic efficiency by three folds compared to pure PVA matrix.

Keywords

PC; PVA-SPEs; Ac-conductivity; Specific capacitance; Photovoltaic efficiency

1. Introduction

Polymer electrolytes are widely used by researchers in various electrochemical devices as they are flexible and versatile in shape. The advantages of using polymeric electrolytes are concentrated on their desirable characteristics: good compatibility with lithium metal; no leakage; low self-discharge in batteries; relaxing elastically under stress and easy processing with continuous production. However, the low ionic conductivity at ambient temperature is one of the major drawbacks of polymer-based solid polymer electrolytes (SPEs) that limit their practical applications [1, 2]. To overcome these problems, solid polymer electrolyte (SPEs) are incorporated with nanocrystals and plasticizers which meets these criteria. Polymer nanocomposite electrolyte was prepared by dispersing the nanoparticles (NPs) such as CuO, ZnO, TiO_2, Al_2O_3, etc., into a complex matrix of polymers and salts [3-6]. The dispersion of NPs and electrolyte salt in the polymeric matrix is an attractive approach due to assist in modifying (i) the local structure/morphology of the matrix (ii) the crystallinity degree (iii) the glass transition temperature (iv) the flexibility of the polymeric segment (v) the chemical properties of the filler particles and (vi) the interaction between heterogeneous systems of nanocrystals/salt and polymers [7]. Besides, one of the useful methods to improve ionic conductivity is the addition of plasticizers as plasticized polymer electrolytes in the solid form [8-12]. The most used plasticizers are low molecular weight organic solvents such as ethylene carbonate (EC), propylene carbonate (PC), dimethyl carbonate (DMC), diethyl carbonate (DEC) and so on [13, 14]. The addition of plasticizer into SPEs leads to enhance the ionic conductivity of 1-2 orders magnitude by increasing flexibility as well as the amorphous content of polymer electrolytes, dissociating salt into free ions, a significant change in morphological structure and lowering the glass transition temperature, Tg [7, 15].

In the current new field, there is always demand for light, safe, and economical devices, so researchers are focusing on the production of such devices whose storage, production and distribution are preferentially at low cost. In this regard, hydrophilic polyvinyl alcohol (PVA) is a potential host polymer having high dielectric strength, good charge storage capacity, high suitable film forming and good mechanical properties [16, 17]. Thus; it has been investigated as they are abundantly available, economical and biodegradable. PVA shows high transparency, compatibility and adhesiveness to the electrode so can be used in electrochemical devices such as cells, sensors, optical devices, etc.

The fine structure of $LiClO_4$ enhances its solubility in the polymer matrix and, eventually, speeds up the salt dissociation process. $LiClO_4$ is used due to its abundant availability, water-soluble and also eco-friendly. Propylene carbonates (PC) have a high

dielectric property and it is a good solvent for electrolyte salt. The plasticizer has an important role towards enhances the segmental motion of PVA chains associated with an increase in the ionic charge carries by increasing the dissociation of electrolyte salt. It restricts the dissociated ions from the salt reforming process and reduces the agglomeration of particles inside the matrix which assist in the performance homogeneity dispersion of components in composite films. Subsequently, the polarization particles inside the composite will increase, reflex in an improve the electrical permittivity and capacity of the stored energy of composite films by reducing the potential barrier in front of the mobility of Li^+ among polymer chains, hence the ionic conductivity will increase. Therefore, the target of the current work is an attempt is made to investigate with enhance the electrical, electrochemical, and optical efficiency of flexible PVA-SPE films and explore the effect of propylene carbonate contents on the features of such films.

2. Experimental Details

2.1 Materials

PVA (average molecular weight 125,000 Aldrich), lithium perchlorate tri hydrate ($LiClO_4.3H_2O$), propylene carbonate as a plasticizer, (PC) ($C_4H_6O_3$) (AR grade, SD. Fine chem.,). Both cesium nitrate ($CsNO_3$), copper (II) nitrate trihydrate [$Cu(NO_3)_2.3H_2O$] (as oxidants) and glycine ($C_2H_5NO_2$) (as fuel) and were purchased from (SD fine-chem, Mumbai, India). Double distilled water was used as a solvent in this study.

2.2 Synthesis Cs_2CuO_2 NPs

In this study, cesium copper oxide Cs_2CuO_2 NPs was synthesized with the sol-gel auto combustion method [18, 19]. AR-grade $Cu(NO_3)_2.3H_2O$, $CsNO_3$, and glycine ($C_2H_5NO_2$; fuel) were weighed in stoichiometric proportions and dissolved in double-distilled water. The molar ratio of the fuel to the oxidant nitrates was 2:1. The individual solutions were then mixed together, and the pH value was adjusted to 8.5 by the addition of NaOH solution. Then, the solution was stirred continuously at 90°C for 2hrs to obtain the gel. The gel was heated until the combustion process occurred, and a loose powder was formed. Finally, the dark grayish brown powder was calcinated at 650-800°C for 2hrs.

2.3 Casting of plasticized PVA-SPEs

PVA of 21g obtained in the powder form was dissolved in 300 ml of doubly distilled water at 80°C for about 2hrs. The 10wt% of $LiClO_4$ was added separately four times into four beakers containing 50 ml of PVA solutions to form polymer electrolyte solutions and then stirred for 1 hr by using a magnetic stirrer at room temperature. Calculated amount viz., 2, 4, 6 and 8wt% of PC and added to the previous solutions separately with continuous stirring for1hr,

then 2wt% of Cs_2CuO_2 NPs added to each of the above-plasticized polymer electrolyte solutions with stirred for 30 min and sonicated for 30min. The plasticized PVA-SPEs were cast in a four petri-dish and the solvent evaporated at room temperature. For complete removal of solvent, the samples were vacuum dried in a hot air oven at 60 ˚C for 4-6 hrs. The thickness of obtained films varied from 0.20 to 0.23 mm. The chemical structure of the pure PVA matrix and the schematic of the composite were depicted in Figure 1.

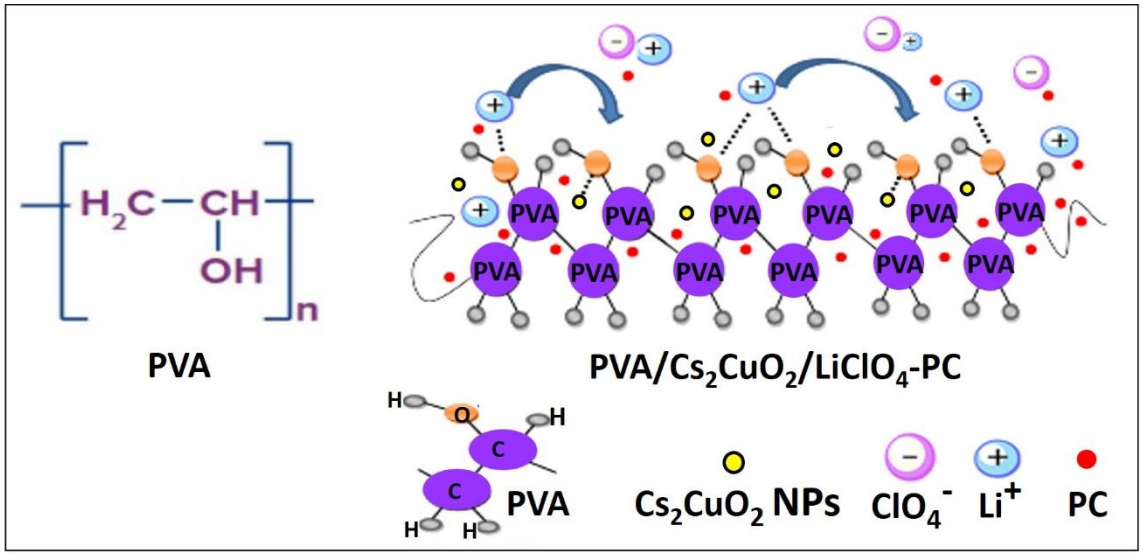

Figure 1. Chemical structure of pure PVA and schematic representation of PVA/Cs_2CuO_2/$LiClO_4$- PC film.

2.4 Techniques

The size of Cs_2CuO_2 NPs was measured by dynamic light scattering (Zetasizer Nano ZS, Malvern Instruments, United Kingdom). The morphological behaviors of plasticized PVA-SPEs were recorded with a Zeiss-108A scanning electron microscope (SEM), in Germany. The structure of pristine Cs_2CuO_2 NPs and plasticized PVA-SPE films were obtained at room temperature by X-ray diffraction (XRD) on a D8 Advance-Bruckers AXS diffractometer with Cu-Kα radiation source (λ = 1.54 ˚A), operated at 40 kV and 40 mA in the 2θ range 10-80˚ at the scan speed of 0.05˚ per second. The physical interaction between components was studied by Fourier transform infrared (FTIR) spectroscopy, JASCO 4100 spectrometer, Japan. All samples scanned over the wave number range 4000-500 cm^{-1}.

The ac-electrical and current-voltage (I-V) features of films were measured by LCR-meter, Wayane Kerr-6430, UK at room temperature. The ac-electrical studies have been carried out in the frequency range 50 Hz-5MHz at 1V. The surface of the films was coated with silver paste and sandwiched between two stainless steel electrodes which had an area of 0.5 cm^2.

Electrochemical cyclic voltammetry (CV) was performed using CH Instrument, model 600D series, with potassium hydroxide (2M) as the background electrolyte at a potential scan rate of 0.1 $V.s^{-1}$, using Ag/AgCl reference and platinum wire as counter electrodes. The photovoltaic (PV) solar-based test system was estimated by Keithley, 2400 digital source meters, Japan with 450 W xenon light source under sun-powered light illumination intensity (60 $mWcm^{-2}$). For the preparation of the photoanode cell, TiO_2 glue was spread over the conducting surface of FTO (1 X 1 cm^2) to make a substrate film of ~ 10 mm thickness.

The dried slide was drenched in a natural pomegranate dye and dried for 2 hrs with a compressed air gun. Another bit of FTO-covered with carbon black. The plasticized PVA-SPE films were immersed in the electrolyte solution (KI/I_2 in ethylene glycol) for 10 min followed by being sandwiched between the two FTO glasses. The sandwiched plasticized PVA-SPEs with two FTO glasses were immersed in electrolyte for a few minutes and then utilized for DSSC studies. The thermal stability of the plasticized SPEs has been studied using thermogravimetric analysis (TGA), TA Instrument Q600, USA, in the temperature range of 30 – 800 ˚C with the heating rate of 15 ˚C/min, in nitrogen gas flow rate of 50 cm^3/min.

3 Results and discussion

3.1 Structural& morphological studies

Figure 2 (a-f) displays the X-ray diffraction (XRD) patterns of pristine Cs_2CuO_2 NPs, pure PVA and different plasticized SPE films. Addition of plasticizer, PC to $PVA/Cs_2CuO_2/LiClO_4$ has been observed to result in an increase in the amorphous nature.

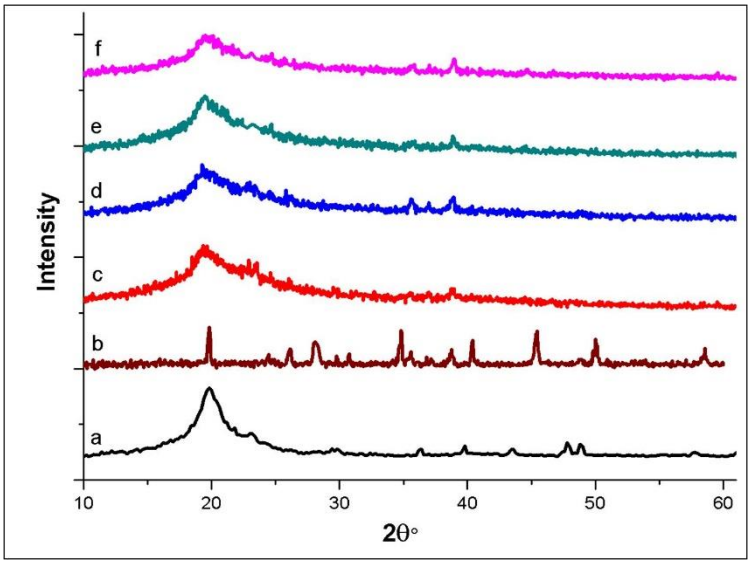

Figure 2. XRD patterns of; a) PVA, b) Cs_2CuO_2 NPs, $PVA/Cs_2CuO_2/LiClO_4$ with c) 2, d) 4, e) 6 and f) 8wt% PC.

As presented in Figure 2(a), PVA has a characteristic peak at 2θ = 19.8° referred to the semi-crystalline nature of PVA [20]. Whereas the pristine Cs_2CuO_2 NPs exhibit multi-sharp crystalline peaks at 2θ of 19.7, 26.1, 28.1, 34.7, 46.2, and 50.18° (Figure 2 (b)). The peaks corresponding to PVA and Cs_2CuO_2 NPs significantly reduced with the addition of PC and $LiClO_4$ in SPEs (Figure 2(c-f)). The addition of PC caused to increase in the dissociation of Li salt, which in turn increases in the interaction between components in SPE films [21]. Therefore, the intensity of the peak at 2θ = 19.8°was decreased and becomes wider in the plasticized PVA-SPE films. Such a decrease in the crystallinity of plasticized PVA-SPE films is in accord with the ionic conductivity results.

Figure 3(a) displays the dynamic light-scattering histogram for the Cs_2CuO_2 NPs, and it reveals that the prepared NPs size was in the range of 80-120nm. The surface morphology and distribution of Cs_2CuO_2 NPs, Li salt and PC in the PVA matrix were characterized using SEM as presented in Figure 3(b-f).

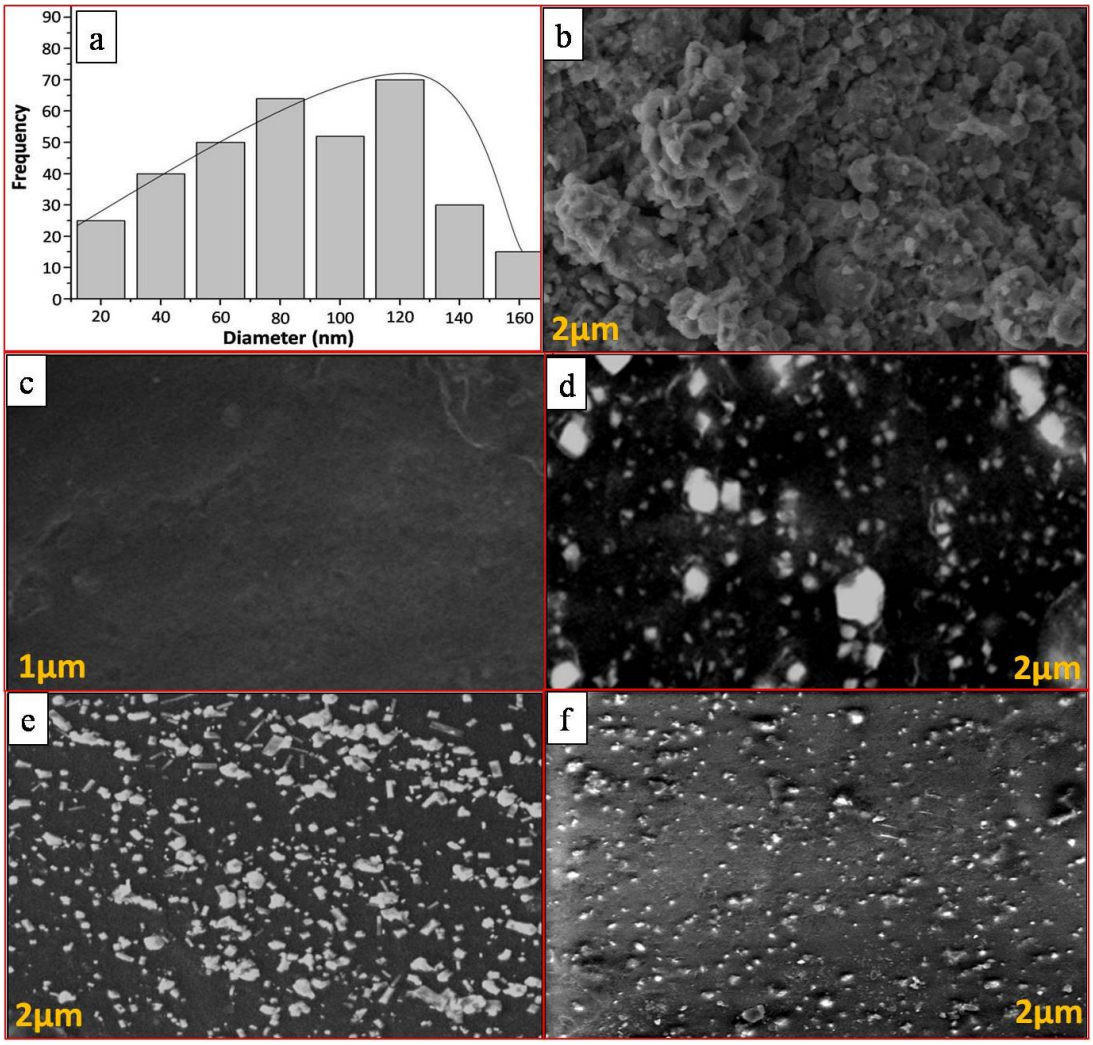

Figure 3. a) Dynamic light-scattering of Cs_2CuO_2 NPs, SEM photomicrographs of; b) pristine Cs_2CuO_2, c) pure PVA, PVA/Cs_2CuO_2/ $LiClO_4$ with d) 2, e) 4 and f) 8wt% PC.

SEM image of the Cs_2CuO_2 NPs shows a porous, agglomerated, and spherical-like structure which was reported else in previous literature [22]. From Figure 3 (c), the SEM image of pure PVA shows a soft surface without any cracks. Besides, the presence of almost spherical NPs and Li salt in the PVA matrix has a uniform distribution with increasing the different amounts of PC in SPEs (Figure 3 (d-f)). These results indicate that the Li salt becomes more dissociation and the NPs have less agglomerated with increasing the PC contents. The addition of PC which has high dielectric constant acts as a solvent for Li salt and prevents NPs from agglomerating in PVA-SPEs. That leads to finer dispersion of fillers in the PVA matrix and the surface of plasticized PVA-SPE films becomes less rough as shown in the films containing 8wt%PC (Figure 3 (e)).

3.2 FTIR analysis

The FTIR analysis provides a powerful means to characterize the complex formation in plasticized PVA-SPE films. Figure 4 displays FTIR spectra for pure PVA and its NCs with 2, 4, 6 and 8 % of PC.

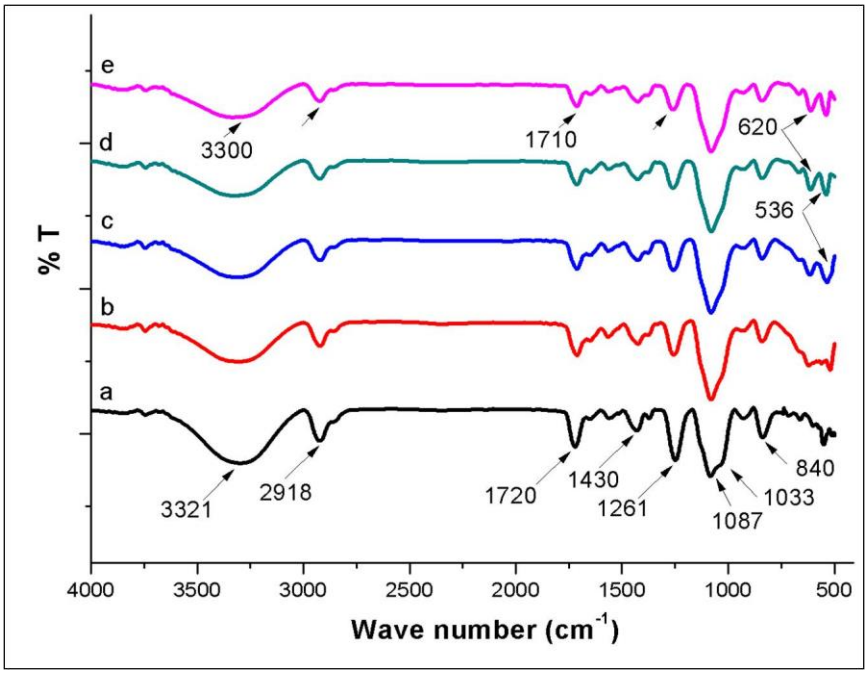

Figure 4. FTIR spectra for a) pure PVA, PVA/Cs_2CuO_2/$LiClO_4$ SPEs with b) 2, c) 4, d) 6 and d) 8wt % of PC.

The reduction in the peak's intensity at 3321, 2918, 1720, 1430, 1260 and 1033 cm^{-1} are assigned to the effect of fillers NPs, Li salt and different amounts of PC [23, 24]. The broad peaks at 3320 and 1087-1033 cm^{-1} referred to the stretching of hydroxyl groups and the single

bond C-O, respectively of the PVA matrix. These peaks exhibited partially changed in plasticized PVA-SPEs. The reducing intensity of both –OH and C-O peaks with the absence of a small shoulder at 1033 cm^{-1} after added PC content confirms the interaction between the fillers and oxygen atoms in the PVA structure.

Further, the intensity of the stretching vibration peak of -CH_2- in PVA-SPEs at 2918 cm^{-1} is decreased because of the existence of Li salt, NPs and PC contents. The reduced intensity of the vibrational peak corresponds to 1720 cm^{-1} with increasing PC content was noticed, which refers to the physical interaction between the carbonyl group of residual acetate groups in the PVA structure with Li^+ of the dissociation salt. A slight decrease of bending vibration in-plane at 1430 cm^{-1} and out-of-plane at 840cm^{-1} of -CH_2 in PVA was observed [25]. There are two peaks were noticed at 620 and 536cm^{-1}, which may be attributed to the effect of inorganic metal oxide NPs [26]. The above observations of reduction in intensity, broadening and shifting of the vibrational peaks confirm the complex formation between Li salt, Cs_2CuO_2 NPs and PVA with increasing the PC contents in SPE films.

3.3 Thermal studies

Figure 5 illustrates the typical thermograms for the decomposition process of PVA and its plasticized PVA-SPE films. The thermal stability revealed through TGA thermograms for plasticized PVA-SPE films is generally significantly lower than that of pure PVA entity. The PVA matrix has adequate stability in the temperature range of 30-330 $^{\circ}$C, then the main decomposition process occurs in the temperature range of 330-500°C, with a weight loss of around 88wt%. From Figure 5, it can be observed that the change in baseline on TGA curves for all PVA-SPE films in the temperature range of 50-200 $^{\circ}$C. It may have referred to the evaporation of adsorbing bulk water and low boiling point components with 6.7wt % loss of pure PVA and 15.6 wt% for 8wt% PC-loaded SPE. As expected, the increasing PC content in the PVA-SPEs causes a reduction in the thermal stability of films accompanied by weight loss from composites at different temperature ranges. Such behavior indicates the incorporated PC into PVA-SPE films leads to a partially reduced thermal stability and the films become flexible and more amorphous. Similar behavior of the effect of plasticizer on the thermal stability of SPE films was published else in the literature [27, 28].

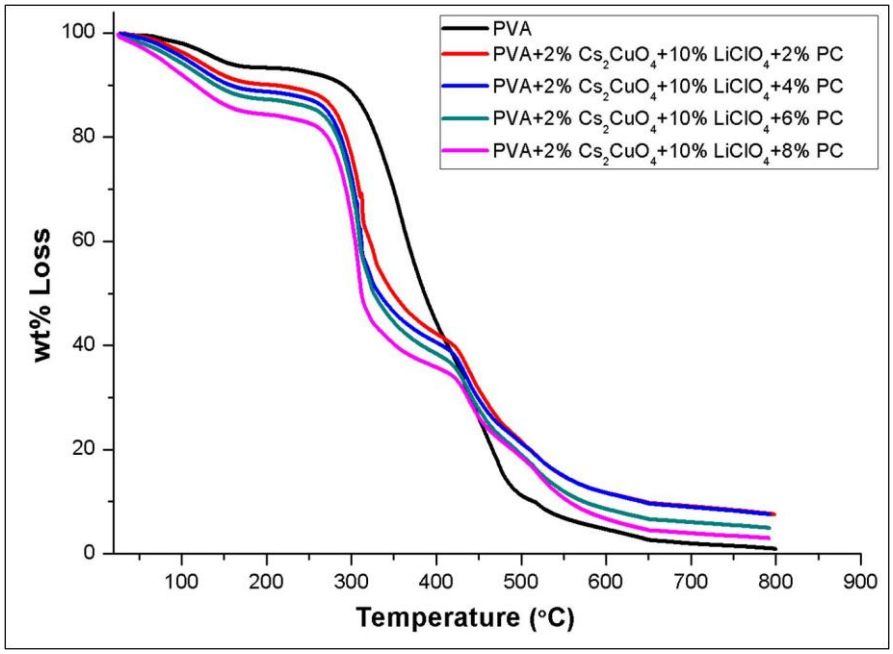

Figure 5. TGA Thermograms of PVA/Cs_2CuO_2/$LiClO_4$-PC versus temperature.

3.4 Electrical and electrochemical behaviors

The ac-conductivity, σ_{ac} versus PC contents in PVA-SPEs at different frequencies and the room temperature were displayed in Figure 6 (a). At lower frequency and less PC content, the σ_{ac} was low. The space charge polarization or impedance of the electrolyte at the electrode/electrolyte interface describes the lower-frequency region of conductivity [29, 30]. In lower frequency regions, the charge carriers are accumulating and stay relatively for a long time at the electrode/electrolyte interface because of the polarization of the electrode. Therefore, the mobility of ions is hindered by these accumulated charges due to columbic repulsion, consequently less ionic conductivity. At higher frequencies, the charge carriers (Li^+ ions) gain more energy and that leads to increasing their mobility through the PVA matrix which becomes more flexible with increasing PC content [31]. As PC content increases, the dissociation of lithium salt will increase means more Li^+ ions will exist, while the viscosity and crystallinity of the PVA matrix will be reduced. Therefore, the segmental motion and flexibility of polymeric chains assist in the transportation of Li^+ ions through the PVA matrix, hence σ_{ac} increase [32]. The maximum σ_{ac} value at higher frequency was found as $9.56X10^{-5}$ S/cm for PVA-SPE doped with 8wt% of PC, however; it is around 0.017, 1.39, 2.21 and 4.95 $X10^{-5}$ S/cm for pure PVA, PVA-SPE doped with 2, 4 and 6wt% of PC, respectively.

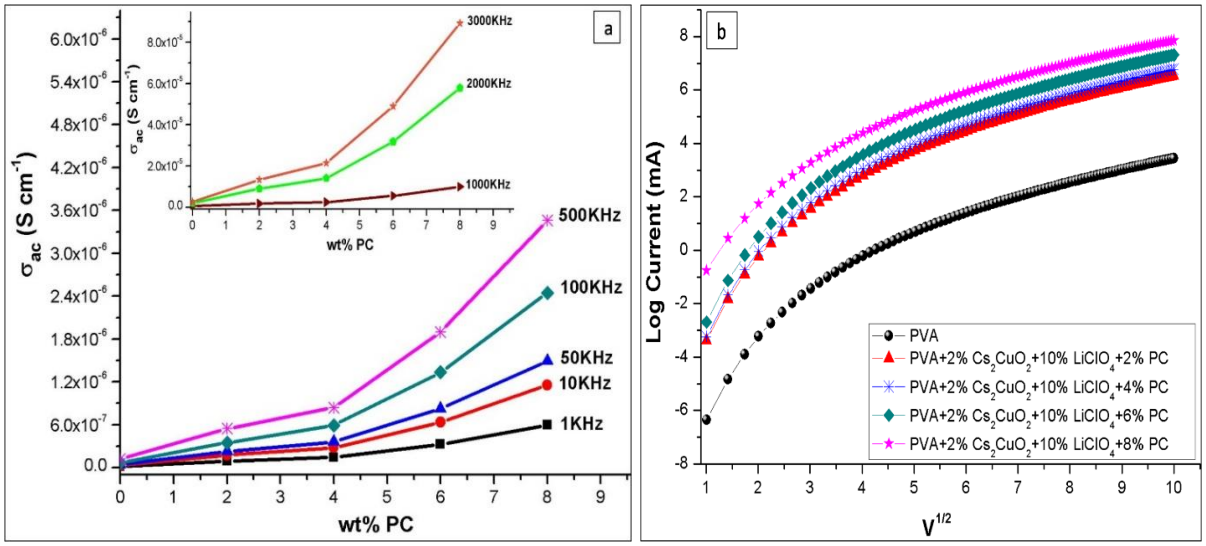

Figure 6. Plots of; a) Ac-conductivity versus PC content at different frequencies and b) Log I versus $V^{1/2}$ of PVA-SPEs.

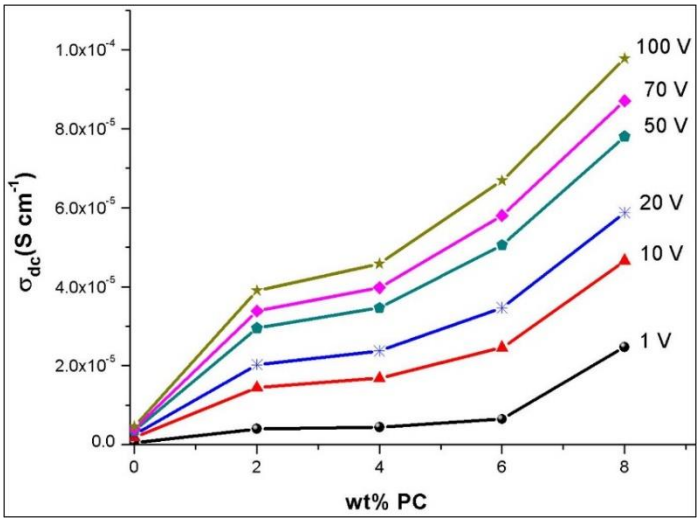

Figure 7. Dc-conductivity versus PC content of PVA-SPEs at different voltages.

Furthermore, in order to determine the exact charge transport mechanism of dc-conductivity in plasticized PVA-SPEs, the plots of log (I) versus ($V^{1/2}$) were plotted as shown in Figure 6 (b). For the Schottky mechanism, the plots of log (I) versus ($V^{1/2}$) should have fit linear plots without deviation [33]. In the current case, the deviation in linearity is observed at below < 4V, therefore the Schottky mechanism was ruled out. Such nonlinear characteristics can arise from transport processes of the number of non-ohmic charge carriers. The deviation of plots may indicate the Poole-Frenkel mechanism, where the transport of charge carriers arises from the electrons of NPs accompanied by the hopping of Li^+ ions through the PVA chains.

Figure 7 showed the dc-conductivity, σ_{dc} dependence on the PC content, which is embedded in PVA-SPE films at room temperature. The increase in σ_{dc} with increasing PC loadings was noticed at different voltages and sharply increases at higher voltages. The increase in PC contents means the small molecules will penetrate into PVA chains and separates them from each other; as a result, the free volume becomes more. That enhances the flexibility and the segmental motion of PVA chains. Besides that, the degree of dissociation of Li salt increases with an increase in the dosage of PC, which leads to enhancement in the σ_{dc}.

Cyclic voltammetry (CV) has been carried out between sweep potential and charge to evaluate the electrochemical stability of the plasticized PVA-SPE films. Figure 8 displayed CV curves of plasticized PVA-SPE films, which have a semi-rectangular shape with a higher current density as compared with pure PVA. The semi-rectangular shape indicates electrochemical stability without decomposition of the films under applied potential voltages.

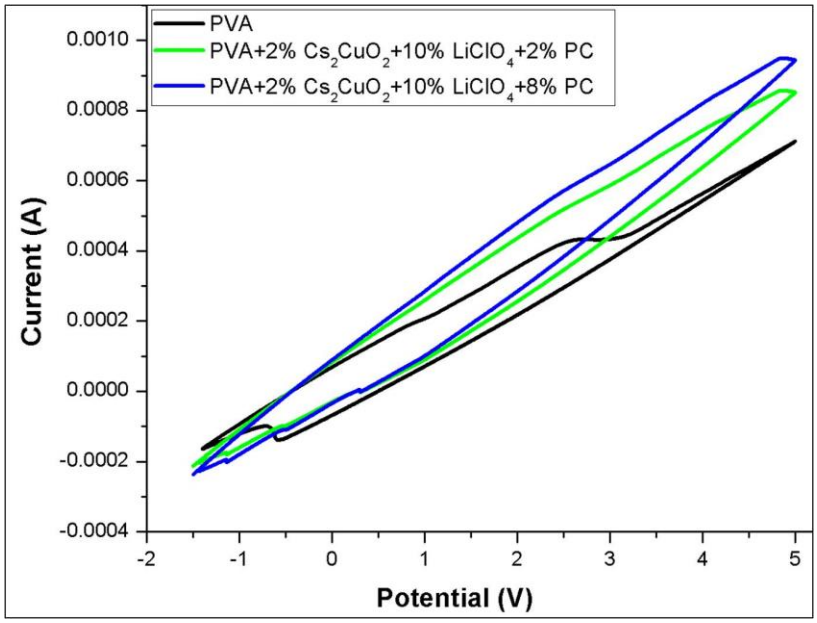

Figure 8. Cyclic voltammetric profiles for PVA and PVA/Cs_2CuO_2/$LiClO_4$-PC SPEs at scan rate of 0.1 $V.s^{-1}$.

The introducing of PC into PVA/Cs_2CuO_2/$LiClO_4$ SPEs leads to producing a flexible film due to the plasticizing effect of PC which also enhances the dissociation of Li salt and the degree of dispersion of fillers. Hence, the interfacial contact is improved leading to an increase in the energy storage of doped films. The improvement of interfacial contact could then induce higher capacitive performance of plasticized SPE films. Furthermore, the ionic conductivity is enhanced upon the addition of a PC which helps in improving the charge storage capacitive behavior. The calculated specific capacitance, C_{spec} of plasticized PVA-SPE films doping with

2 and 8wt% of PC are 3.73 and 4.17 F/g, respectively which is higher than that of pure PVA (2.11F/g). That indicates the addition of PC to PVA-SPE films enhances its capacitance values. The obtained data of the C_{spec} of plasticized PVA-SPE films is higher by two folds compared with the C_{spec} of other PVA nanocomposites reported else [34, 35].

3.5 Photovoltaic activity

Figure 9 shows the photocurrent density-voltage curves for the dye-sensitized solar cells (DSSCs) created for pure PVA and PVA-SPEs containing 2,4 and 8wt% of PC.

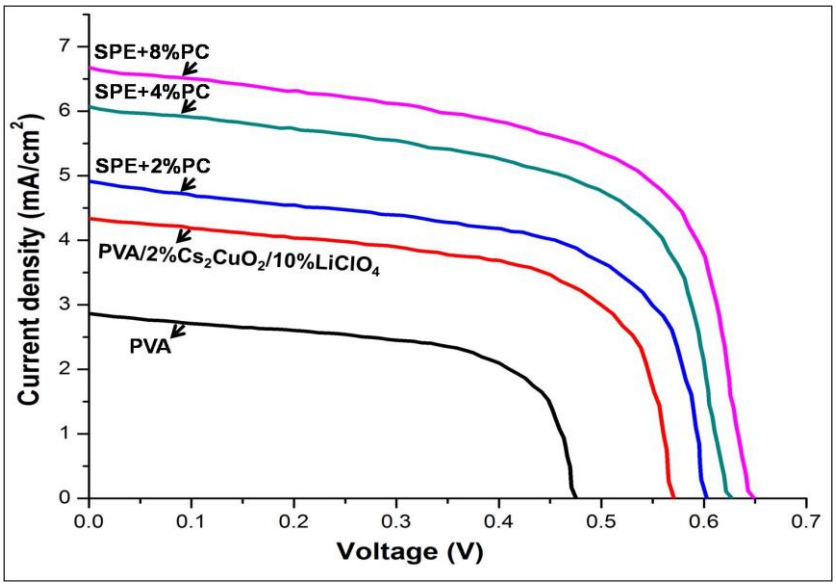

Figure 9. Current density-voltage of pure PVA and PVA/Cs_2CuO_2/$LiClO_4$-PC SPEs in KI/I_2 electrolyte based DSSC under illumination intensity of 60 mW/cm^2.

The Photovoltaic parameters based on DSSCs as the fill factor (*FF*) and the power conversion efficiency (η) for PVA-SPEs were obtained from Eq.1 as follows.

$$FF = \frac{I_{mp} \times V_{mp}}{I_{SC} \times V_{OC}} \quad , \quad \eta(\%) = \frac{FF \times I_{SC} \times V_{OC}}{P_{in}} \times 100\% \qquad (1)$$

Where V_{oc} is the open circuit voltage (V), I_{sc} is the short circuit current density (mA/cm^2), P_{in} is the incident light power, I_{mp} (mA/cm^2) and V_{mp} (V) are the current density and voltage at the maximum point of power output (P_{max}), respectively. The calculated photovoltaic parameters for PVA and PVA-SPE films were listed in Table 1.

Table 1: Photovoltaic parameters of PVA and PVA/Cs2CuO2/LiClO4-PC SPEs based DSSC.

Composition	I_{sc} (mA)	V_{oc} (V)	P_{max}		FF	% FF	% η*
			I_{mp}	V_{mp}			
PVA	2.881	0.471	1.813	0.421	0.562	56.2	1.27
PVA/2%Cs_2CuO_2/10%$LiClO_4$	4.359	0.567	3.316	0.461	0.618	61.8	2.54
PVA/2%Cs_2CuO_2/10%$LiClO_4$+2%PC	4.934	0.601	3.725	0.494	0.621	62.1	3.06
PVA/2%Cs_2CuO_2/10%$LiClO_4$+4%PC	6.106	0.623	4.497	0.538	0.636	63.6	4.03
PVA/2%Cs_2CuO_2/10%$LiClO_4$+8%PC	6.701	0.630	4.791	0.566	0.642	64.2	4.51

*% η is calculated at P_{in} = 60 mW/cm^2.

The results reveal drastic increases in the *FF* and *η* values for the PVA-SPE containing different dosages of PC contents compared to the pure PVA matrix. The increases of *FF* and *η* denote the increase of I_{sc} values through the cell as can be seen in Table 1. The incorporation of 2wt% of Cs_2CuO_2 NPs and10%wt of $LiClO_4$ into the PVA matrix will improve its response towards the absorption of the light and will build a network or conduction path through PVA which facilitates the transportation of charge carriers through it. These movements of charge carriers will aid to separate the opposite charges through the cell. It is clearly noticed that increasing the PC contents in PVA-SPEs leads to an increase in the dissociation of Li salt and will prevent them from reforming salt again as well as restraining the agglomerate of Cs_2CuO_2 NPs in the matrix. The flexibility of PVA-SPEs also will be enhanced after the addition of PC caused to assist the transportation of charge carriers. Besides, the plasticized PVA-SPEs have higher conductivity compared to the insulating pure PVA. Therefore, the plasticized PVA-SPEs have higher *FF* and *η* values than other formulations. Additionally, the higher ionic mobility of iodide ions of electrolyte and the faster re-excited of the electrons from HUMO to LUMO from the dye orbital leads to improvement in the efficiency of the cell. The *η* value of pure PVA (1.27 %) in iodide electrolyte in this study is very close to that for pure PVA/KI/I_2 (1.97 %) reported in the literature [36, 37]. While the *η* value of PVA-SPE containing 8wt% of PC (4.51 %) is higher by one-fold than that of PVA/4 wt% α-Fe_2O_3 (3.62 %) NC in the KI/I_2, published elsewhere [38, 39]. Such outcomes demonstrate that the plasticized PVA-SPEs can be improved to widen their potential application as a promising flexible material for DSSCs.

4 Conclusions

The plasticized PVA-SPEs containing different dosages viz., 2, 4, 6 and 8 wt% of PC as a plasticizer have been fabricated by the solution-casting method. The XRD and SEM analysis confirmed a significant microstructural variation and uniform dispersion of fillers in SPEs respectively, whereas the dispersion becomes more ideal with increasing PC content in SPE films. FTIR spectroscopy further established that the incorporation of varying amounts of PC in SPEs changes the vibration stretching peaks of main groups in the PVA matrix as a result of increasing the ion-dipole interactions. The ac and dc conductivity increases with increasing the frequency and PC contents in PVA-SPEs. The Pool-Frenkel mechanism associated with the ions hopping is found to be the dominant conduction mechanism responsible for charge transport. In plasticized PVA-SPE films, the interfacial contact between electrode-electrolyte and mobility of ions leads to enhance their specific capacitance. TGA studies revealed that the addition of 8 wt% PC in the NC films shifts the thermal decomposition temperature to a lower value. The photovoltaic efficiency of plasticized PVA-SPEs increases by two folds compared with pure PVA and that may be adjustable to widen their potential application in DSSCs.

References

[1] Cha E. H., Macfarlane D. R., Forsyth M. and Lee C. W., (2004) Ionic Conductivity Studies of Polymeric Electrolytes Containing Lithium Salt with Plasticizer, *Electrochimica Acta* **50:** 335-338.

[2] Jinisha B., Anilkumar K. M., Manoj M., Pradeep V. S. and Jayalekshmi S., (2017) Development of A Novel Type of Solid Polymer Electrolyte for Solid State Lithium Battery Applications Based On Lithium Enriched Poly (Ethylene Oxide) (PEO)/Poly (Vinyl Pyrrolidone) (PVP) Blend Polymer, *Electrochimica Acta* **235:** 210-222.

[3] Arup D., Kajari D. S., Karan S. and De K. (2011) Vibrational Spectroscopy And Ionic Conductivity of Polyethylene Oxide–$NaClO_4$–CuO Nanocomposite, *Spectrochimica Acta Part A: Molecular and Biomolecular Spectroscopy* **83:** 384-391.

[4] Patil S. U., Yawale S. S. and Yawale S. P. (2014) Conductivity Study of PEO–$LiClO_4$ Polymer Electrolyte Doped with ZnO Nanocomposite Ceramic *Filler*, *Bulletin of Materials Science* **37:** 1403-1409.

[5] Vignarooban K., Dissanayake M.A.K.L., Albinsson I. and Mellander B. E. (2014) Effect of TiO_2 Nano-Filler And EC Plasticizer on Electrical And Thermal Properties of Poly(Ethylene Oxide) (PEO) Based Solid Polymer Electrolytes, *Solid State Ionics* **266:** 25-28.

[6] Das S. and Ghosh A. (2015) Ion Conduction and Relaxation in PEO-LiTFSI-Al_2O_3 Polymer Nanocomposite Electrolytes, *Journal of Applied Physics* **117:** 174103 (1-7).

[7] Pradan D.K., Samantaray B.K., Choudary R. N. P. and Thakur A.K. (2005) Effect of Plasticizer on Structure-Property Relationship in Composite Polymer Electrolytes, *Journal of Power Sources* **139**: 384-393.

[8] Xiaofei M., Jiugao Y., and Wang N. (2007) The Effects of Different Plasticizers on the Properties of Thermoplastic Starch as Solid Polymer Electrolytes, Macromolecular *Materials and Engineering* **292:** 503-510.

[9] Pradhan D. K., Choudhary R. N. P., K.Samantaray B., Karan N. K. and Katiyar R. S. (2007) Effect of Plasticizer on Structural and Electrical Properties of Polymer Nanocompsoite Electrolytes, *International Journal of Electrochemical Science* **2:** 861-871.

[10] Pitawala H. M. C., Dissanayake M. A. L., Seneviratne V. A., Mellander B. E. and Albinson I. (2008) Effect of Plasticizers (EC or PC) on The Ionic Conductivity and Thermal Properties of the $(PEO)_9LiTf:Al_2O_3$ Nanocomposite Polymer Electrolyte System, J. Solid State Electrochemistry **12:** 783-789.

[11] Pawlicka A., Danczuk M., Wieczorek W. and Monikowska E.Z. (2008) Influence of Plasticizer Type on The Properties of Polymer Electrolytes Based on Chitosan. *The Journal of Physical Chemistry A* **112**: 8888-8895.

[12] Sasithorn K. and Jantrawan P. (2015) Effects of Nano Alumina and Plasticizers on Morphology, Ionic Conductivity, Thermal and Mechanical Properties of PEO-$LiCF_3SO_3$ Solid Polymer Electrolyte, *Electrochimica Acta* **161**:171-176.

[13] Zhao H., Park S. J., Feifei S., Yanbo F., Battaglia V., Philip N. R. J. and Liu G. (2014) Propylene Carbonate (PC)-Based Electrolytes with High Coulombic Efficiency For Lithium-Ion Batteries, *Journal of the Electrochemical Society* **161**: 194-200.

[14] Shukur M. F., Majid N. A., Ithnin R. and Kadir M. F. Z. (2013) Effect of Plasticization on the Conductivity and Dielectric Properties of Starch–Chitosan Blend Biopolymer Electrolytes Infused with NH_4Br, *Physica Scripta* **157**: 014051(1-6).

[15] Anupama B.H., Murad Q. A. A, Shashikala B.S., Somesh T.E., Kavya R., Siddaramaiah and Madhukar B.S. (2023) Poly (O-Anicidine) Encapsulated K_2ZrO_3 Nano-Core Based Gelatin Nanocomposites: Investigation of Optical, Thermal, Microcrystalline and Morphological Characteristics, *Chemistry Select* **7**: 1-12.

[16] Rajeswari N., Selvasekarapandian S., Karthikeyan S., Sanjeeviraja C., Iwai Y. and Kawamura J. (2013) Structural, Vibrational, Thermal, and Electrical Properties of PVA/PVP Biodegradable Polymer Blend Electrolyte with CH_3COONH_4, *Ionics* **19**: 1105-1113.

[17] Radha K., Selvasekarapandian S., Karthikeyan S., Hema M. and Sanjeeviraja C. (2013) Synthesis and Impedance Analysis of Proton-Conducting Polymer Electrolyte PVA:NH_4F, *Ionics* **19**: 1437-1447.

[18] Murad Q.A.A., Adel M.N.S., Subramani N.K., Madhukar B. S. and Siddaramaiah (2017) Optical Parameters, Electrical Permittivity and I-V Characteristics of PVA/Cs_2CuO_2 Nanocomposite Films for Opto-Electronic Applications, *Journal of Materials Science: Materials in Electronics* **28**: 8074-8086.

[19] Anupama B.H., Murad Q.A. A. and Siddaramaiah (2021) Performance of Nano-K-doped Zirconate On Modified Opto-Electrical and Electrochemical Properties of Gelatin Biopolymer Nanocomposites, *Polymer Bulletin* **78**: 3023-3041.

[20] Somesh T. E, Murad Q.A. A., Madhukar B.S. and Siddaramaiah (2018) Photosensitization of Optical Band Gap Modified PVA Films with Hybrid $AgAlO_2$ Nanoparticles, *Journal of Materials Science: Materials in Electronics* **30**: 37-49.

[21] Sharma J. P. and Sekhon S. S. (2013) Effect of Plasticizer and Fumed Silica on Ionic Conductivity Behavior of Proton Conducting Polymer Electrolytes Containing HPF_6, *Bulletin of Materials Science* **36:** 629-634.

[22] Murad Q.A. A., Adel M. N. S. and Siddaramaiah (2018) Effects of the Electrolyte Content on The Electrical Permittivity, Thermal Stability, and Optical Dispersion of Poly (Vinyl Alcohol)–Cesium Copper Oxide–

Lithium Perchlorate Nanocomposite Solid-Polymer Electrolytes, *Journal of Applied Polymer Science* **135**: 45852(1-14).

[23] Osman Z., Ansor N. M., Chew K.W. and Kamarulzaman N. (2005) Infrared and Conductivity Studies on Blends of PMMA/PEO Based Polymer Electrolytes, *Ionics* **11**: 431-435.

[24] Adel M.N S., Murad Q.A. A. and Siddaramaiah (2018) Effect of Lithium Perchlorate on the Optoelectrical and Thermal Properties of Poly (Vinyl pyrrolidone)/Nano-Cesium Aluminate Solid Polymer Electrolytes, *Polymer Plastics Technology and Engineering* **57**: 1554-1566.

[25] Papke B.L., Ratner M. A. and Shriver D. F. (1981) Vibrational Spectroscopy and Structure of Polymer Electrolytes, Poly (Ethylene Oxide) Complexes of Alkali Metal Salts, *Journal of Physics and Chemistry of Solids* **42**: 493-500.

[26] Karthik K., Victor J., Kanagaraj M. and Arumugam S. (2011) Temperature-Dependent Magnetic Anomalies of CuO Nanoparticles, *Solid State Communications* **151**: 564-568.

[27] Adel M. N. S., Hezam A., Murad Q. A. A., Somesh T.E. and Siddaramaiah (2020) Effect of Ethylene Carbonate on Properties of PVP-$CsAlO_2$-$LiClO_4$ Solid Polymer Electrolytes, *Polymer-Plastics Technology and Materials* **60**: 132-146.

[28] Murad Q. A. A., Shashikala B.S., Gayitri H.M., Khaled A., Nabil A., Ahmed B. and Fares H. A. A. (2022) Characterization of Opto-Electrical, Electrochemical and Mechanical Behaviors of Flexible PVA/(PANI+La_2CuO_4)/$LiClO_4$-PC Polymer Blend Electrolyte Films, *Macromolecular Research* **30**: 1-9.

[29] Ramesh S., Yin T. S. and Liew C-W. (2011) Effect of Dibutyl Phthalate as Plasticizer on High Molecular Weight Poly (Vinyl Chloride) Lithium Tetraborate Based Solid Polymer Electrolytes, *Ionics* **17**: 705-713.

[30] Murad Q.A. A., Adel M.N.S., Gayitri H. M. and Siddaramaiah (2020) Impact of Nano-Perovskite La_2CuO_4 on Dc-Conduction, Opto-Electrical Sensing and Thermal Behavior of PVA Nanocomposite Films, *Polymer-Plastics Technology and Materials* **59**: 469-483.

[31] Elias S. and Mohd A. M. (2006) Effect of Radiation on Conductivity of Solid PVA–KOH–PC Composite Polymer Electrolytes, *Ionics* **12**: 53-56.

[32] Rajendran S., Sivakumar M., Subadevi R. (2004) Investigations on The Effect of Various Plasticizers in PVA-PMMA Solid Polymer Blend Electrolytes, *Materials Letters* **58**: 641-649.

[33] Murad Q.A. A., Somesh T.E, Gayitri H.M, Fares H. Al-Ostoot and Siddaramaiah (2020) Optimized Nano-Perovskite Lanthanum Cuprate Decorated PVA Based Solid Polymer Electrolyte, *Polymer-Plastics Technology and Materials* **59**: 215-229.

[34] Gayitri H. M., Murad Q.A. A., Siddaramaiah, and Gnana P. A. P. (2020) Investigation of Triplex $CaAl_2ZnO_5$, Nanocrystals on Electrical Permittivity, Optical and Structural Characteristics of PVA Nanocomposite Films, *Polymer Bulletin* **77**: 5005-5026.

[35] Gayitri H. M., Murad Q. A. A., Fares H. A., Nabil A., Ahmed B., and Gnanaprakash A.P. (2023) Investigation on Opto-Electrical Structural And Electrochemical Performance of PVA/$ZnBi_2MoO_7$ Hybrid Nanocomposites, *Polymer Bulletin* **80**: 773-790.

[36] Arof A. K., Naeem M., Hameed F., Jayasundara W. J. M., Careem M. A., Teo L. P. and Buraidah M. H. (2014) Quasi Solid State Dye-Sensitized Solar Cells Based On Polyvinyl Alcohol (PVA) Electrolytes Containing I^-/I^{-3} Redox Couple, *Optical and Quantum Electronics* **46**: 143-154.

[37] Shashikala B. S., Murad Q.A. A., Somesh T.E, Siddaramaiah and Anasuya S. J. (2022) Core-Shell Synergistic Effect of (PANI-$NaBiO_2$) Incorporation Polycarbonate Films to Photodegradation of MG Dye and Photovoltaic Activity, *Polymer Bulletin* **79**: 7531–7554.

[38] Senthil R. A., Theerthagiri J. and Madhavan J. (2015) Hematite Fe_2O_3 Nanoparticles Incorporated Polyvinyl Alcohol Based Polymer Electrolytes for Dye-Sensitized Solar Cells. *Materials Science Forum* **832**: 72-83.

[39] Shashikala B.S., Murad Q.A. A., Fares H. A., Nabil A., Ahmed B., Siddaramaiah, and Anasuya S. J. (2022) Probing Optical Efficiency and Electrochemical Behaviors of Polycarbonate Incorporating Conducting PANI and Halloysite Nanotube (HNTs) as Core-Sell Nanofillers, *Polymer Bulletin* **79**: 10333-10355.

TUJNAS
ISSN-Print: 2073-0764
ISSN-Online: 2959-4340

Thamar University Journal of
Natural & Applied Sciences
(TUJNAS)

Journal website:
www.tu.edu.ye/journals/index.php/TUJNAS/index

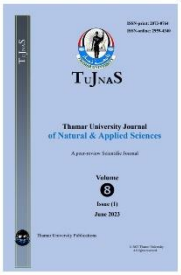

ORIGINAL ARTICLE

Synthesis, Structural, Optical and Electrical Properties of Pure and Doped NiO Nanostructures Prepared via The Co-precipitation Method

Enas Ali Ahmed Alahsab, Abdullah A. A. Ahmed*, A. M. Abdulwahab

Affliations:
Department of Physics, Faculty of Applied Science, Thamar University, Dhamar 87246, Yemen.

Corresponding Author:
Abdullah A. A. Ahmed, emails: abdullah2803@gmail.com or abdullah2803@tu.edu.ye

Received: May 12, 2023,

Revised Date: Jun 6, 2023,

Accepted Date: Jun 12, 2023,

Online Date: Jun 13, 2023

Published: Jun 13, 2023

DOI:
https://doi.org/10.59167/tujnas.v8i1.1491

Abstract

Here, we report the synthesized high purity NiO nanostructures using simple and inexpensive chemical route. NiO NPs and (Cu, Zn) single and dual doped NiO NPs prepared by co-precipitation technique and annealed at 350 ℃ for 2 hours. Structural properties of prepared samples were investigated by X-ray diffraction (XRD). The optical characterizations and electrical conductivity were characterized by UV-vis spectrophotometer and I-V measurement. The crystallite size for dual doped NiO samples was 7.9 ± 0.9 nm compared to pure NiO, which had 9.52 nm. These results are consistent with the ionic radii of the doped metals. The obtained values of the band gap energy increased from 3 eV for pure sample to higher values (3.14 ± 0.06 eV) for doped samples due to the quantum confinement effect. These results agreed with the DC conductivity of samples. The ionic conductivity σ_{ionic} was developed with dual doping. The characterization of the doped samples makes them good candidates for photoelectronic applications.

Keywords

Nickel oxide nanostructures; Dual doping; Band gap energy; Electrical properties

1. Introduction

Nickel oxide (NiO) is a green crystalline solid material with ferromagnetic properties and a Neel temperature of 523 K. NiO has unique electrical, magnetic, and optical properties that make it the primary subject of numerous applications. NiO is a material with extreme chemical stability. Due to its low cost and excellent ion storage property, it has become an interesting research material [1]. NiO NPs is a p-type conductivity due to its wide energy band gap from 3.6 eV to 4.0 eV [2, 3]. There are several methods to synthesis of NiO NPs such as electro deposition (ED), hydrothermal method [4] Sol-gel, thermal decomposition and Chemical precipitation [1, 5, 6]. NiO nanoparticles can be used in various applications like photocatalytic, battery, electrochromic, chemical sensing applications [7-9] and gas sensor application [4].

The doped NiO NPs lead to improvement of physical properties for various applications. K Varunkumar *et al.,* reported on Cu doped NiO NPs prepared by co-precipitation and studied optical and thermal stability, the bandgap increased from 3.32 to 3.37 eV at 8 (wt %) and showed exhibit good thermal stability [10]. K. Varunkumar *et al.,* studied morphology of the pure NiO and Cu doped NiO NPs at different calcination temperatures 350 °C, 450 °C and 550 °C that revealed spherical shaped particles for pure NiO and Cu doped NiO samples calcined at 350 °C while changes were observed for other calcination temperatures [11]. Zn doped NiO nanoparticles were synthesized by co-precipitation method at calcination temperature of 550˚C and the optical band gap was found at 3.26 eV [12]. Solvothermal synthesis of pure and Zn doped NiO nanocluster electrocatalysts resulted in higher conductivity with lower internal resistance (Rs) of 10.36 Ω for the above optimized electrocatalyst [9]. Recently, Zn-doped NiO thin films were synthesized for highly sensitive and selective ammonia sensors [13].

In the present study, pure, single and dual (Cu and Zn) doped NiO nanoparticles were synthesized by co-precipitation method and structure, optical and electrical properties of the prepared samples were reported.

2. Experimental Details

2.1 Materials

Nickel nitrate hexahydrate $Ni(NO_3)_2.6H_2O$ (Fluka, ≥ 98%), copper nitrate trihydrate $Cu(NO_3)_2.3H_2O$ (Scharlau, extra pure), zinc nitrate hexahydrate $Zn(NO_3)_2.6H_2O$ (Fluka. ≥ 98%) and sodium hydroxide (95%). The solvent used for all mentioned chemicals was distilled water.

2.2 Synthesis of pure NiO Nanostructures

1 M nickel nitrate solution was prepared by dissolving 14.54 g in 50 ml distilled water with constant stirring for 20 min. 0.1 M NaOH was added dropwise to the nickel nitrate solution to adjust the pH to 10 and stirred at room temperature for 3 h until a light green colored solution was obtained. The final solution was kept in an airtight container for one day to obtain the precipitate, which was centrifuged at 4000 rpm for 15 minutes and then washed several times with distilled water. The collected precipitate was dried at 80 ℃ for 15 h and then ground into fine powder with mortar and pestle. Finally, the powder was annealed at 350 ℃ for 2 h to obtain a pure NiO nanostructure.

2.3 Synthesis of Cu-Zn dual doped NiO Nanostructures

Copper nitrate and zinc nitrate solutions were prepared separately in 5 concentrations (0.025, 0.05, 0.075 and 0.1 M). The mixing of different solutions was clarified in Table 1 to obtained single and dual doped NiO according to the formula $Ni_{0.9}(Cu_{1-x}Zn_x)_{0.1}O$, where x = 0, 0.25, 0.5, 0.75 and 1. As presented in Table 1, there were two single doped NiO samples at x = 0 (Cu only) and one (Zn only) and 3 dual doped NiO samples (at x = 0.25, 0.5 and 0.75). x value indicated to the increase of Zn doped percentage in NiO from 0 to 0.1 as x value increased from 0 to 0.01 and decreasing of Cu doped percentage in the same time from 0.1 to 0.

0.9 M of nickel nitrate solution was prepared in 75 ml of distilled water under constant stirring for 20 min and labeled as solution (A). For sample prepared at x = 0.25, 0.025 M zinc nitrate and 0.075 M copper nitrate solutions were prepared separately in 75 ml of distilled water under constant stirring for 20 min and labeled as solution (B) and (C), respectively. Solutions A, B and C were mixed under constant stirring for further hour at RT. The pH value of the mixed solutions was adjust to 10 by addition of 0.1 M NaOH drop by drop under constant stirrer for 3 h at RT. The light green solution was obtained and kept in an airtight container for a day to collect the precipitate. The precipitate was filtered and centrifuged at 4000 rpm for 15 min and then washed with distilled water several times. The final precipitate was dried in oven for 15 h at 80℃. Then it was grind using mortar and pestle to get fine powder and finally, powder was annealed at 350 ℃ for 2 h to obtain $Ni_{0.9}Cu_{0.075}Zn_{0.025}O$ nanostructure. The other samples were prepared by repeating of the above procedures for all x values according to arranged concentrations in Table 1.

2.4 Characterizations

The structural properties of prepared samples have investigated using the X-ray diffraction (XRD) technique (XD-2 X-ray diffractometer using CuKα (λ = 1.54 Å) at 36 kV and 20 mA, China) in Yemeni Geological Survey and Minerals Resources Board (YGSMRB).

The absorbance and transmittance spectra of samples were measured using a UV–VISIBLE spectrophotometer (SPECORD 200) at room temperature in the wavelength range of (190–1100 nm). The diluted hydrochloric (HCl) acid was used as a solvent for prepared samples to measure the absorbance and transmittance spectra. The powder of all prepared samples was pressed into pellet forms with a thickness of about 1 mm and a diameter of 13 mm using a Carver hydraulic press machine. These pellets were used to measure the DC electrical conductivity at room temperature.

Table 1: Experimental details for preparation of single and dual doped NiO nanostructures.

Samples	Concentrations in (M)			Doping type	x value
	Nickel nitrate (doping %)	Copper nitrate (doping %)	Zinc nitrate (doping %)		
$Ni_{0.9}Cu_{0.1}O$	0.9	0.1 (10%)	- (0%)	Single	x = 0
$Ni_{0.9}Cu_{0.075}Zn_{0.025}O$	0.9	0.075 (7.5%)	0.025 (2.5%)	Dual	x = 0.25
$Ni_{0.9}Cu_{0.05}Zn_{0.05}O$	0.9	0.05 (5%)	0.05 (5%)	Dual	x = 0.5
$Ni_{0.9}Cu_{0.025}Zn_{0.075}O$	0.9	0.025 (2.5%)	0.075 (7.5%)	Dual	x = 0.75
$Ni_{0.9}Zn_{0.1}O$	0.9	- (0%)	0.1 (10%)	Single	x = 1

3 Results and discussion

3.1 X-ray diffraction (XRD)

Figure 1 shows three distinct pattern planes (111), (200), and (220) of the NiO phase, confirming that the NiO form in cubic structure is consistent with the standard card no. (JCPDS card No. 44-1159). The XRD patterns show pure NiO, single and dual doped NiO nanostructures. This means that dual doping does not change the structure of the NiO nanostructures. The XRD patterns of the prepared samples are calculated according to the following equations [14-16] in Table 2:

$$\frac{1}{d^2} = \frac{(h^2+k^2+l^2)}{a^2} \quad (1)$$

$$D = \frac{k\lambda}{\beta \cos\theta} \quad (2)$$

$$\varepsilon = \frac{\beta_{hkl}}{4\tan\theta} \quad (3)$$

Where d_{hkl} is the interplanar space and (h, k and l) are Miller indices. β is the full width at half maximum (FWHM) of the diffraction peak (200), (λ) is the wavelength of X-ray (λ = 0.154nm) and (θ) is the half angle Bragg diffraction. The low intensity of the XRD patterns for undoped and doped NiO nanostructures (Figure 1) indicates that the samples have low crystallinity due to the nano range of the crystallite size of the prepared samples. Figure 1 shows the XRD patterns of copper and zinc dual doped nickel oxide nanostructures ($Ni_{0.9}(Cu_{1-x}Zn_x)_{0.1}O$) at x= 0, 0.25, 0.5, 0.75 and 1. When x= 0 ($Ni_{0.9}Cu_{0.1}O$), 2θ value of (200) crystal face that showed shifting of diffraction peaks to the lower angle from $43.192^{\circ}$for pure NiO to 43.07° for $Ni_{0.9}Cu_{0.1}O$ sample is predicted as a result of increase lattice constants [14]. Full width at half maximumat β (FWHM) at plane (200) also increase from 0.898° for pure to 1.212° for $Ni_{0.9}Cu_{0.1}O$. The increase in β is due to expansion of the crystal structure as the slightly larger ionic radius of Cu^{2+}(0.73A°) substituted that of Ni^{2+}(0.69A°) in NiO cubic structure [14]. The crystallite size decrease from 9.52 nm for pure NiO to 7.05 nm for $Ni_{0.9}Cu_{0.1}O$ this reduction in the crystallite size for the doped nanoparticles could be attributed to the internal microstructural strain and disorder introduced in the NiO lattice due to incorporation of the Cu ion, this result was in good agreement that published in this literature [11].

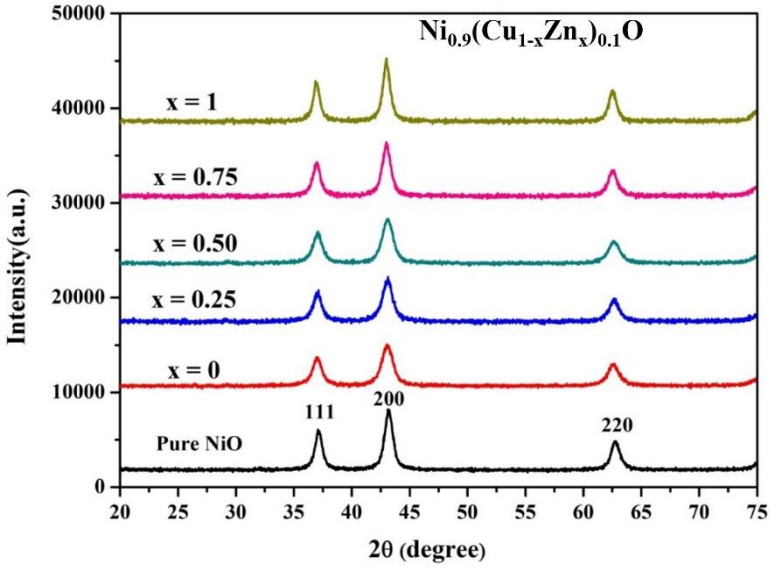

Figure 1. XRD patterns of undoped and doped NiO nanostructures.

For dual doped sample at x = 0.25 ($\mathbf{Ni_{0.9}Cu_{0.075}Zn_{0.025}O}$), **2θ** value of (200) diffraction also shifting to the lower angle by 0.102 due to both dual $\mathbf{Cu^{2+}}$(0.073 nm) and $\mathbf{Zn^{2+}}$(0.074 nm) dopants have larger ionic radii than $\mathbf{Ni^{2+}}$ ions (0.069 nm) [15]. ***β*(FWHM)** ($\mathbf{1.122}^{\circ}$) stilled higher than the pure NiO sample which confirm the substitution of $\mathbf{Ni^{2+}}$ ions

by both $\mathbf{Cu^{2+}}$and $\mathbf{Zn^{2+}}$ ions. The shifting to the lower angle were observed for the other dual samples (x =0.5 and 0.75) as listed in Table 2 due to the same reason mentioned above. But at ($\mathbf{Ni_{0.9}Zn_{0.1}O}$) the shifting to the lower angle , the crystallite size of NiO and Zn doped NiO increased from 9.52 to 10.27 nm due to $\mathbf{Zn^{2+}}$ ions have a large ion radius of 0.074 nm compared to the ionic radius of $\mathbf{Ni^{2+}}$ [16]. The discrepancy between the increase and decrease in the values of microstrain caused with increase in the value of x in structural distortion and cell volume narrowing according to the difference of concentrations. Variation in microstrain may be due to the change in microstructure, size and shape of the particles [16]. In Table 2 the lattice parameter ($\mathbf{a_{hkl}}$), microstrain (ε) and crystallite size (D) values are shown.

Table 2: The structural measurements of prepared samples from (200) diffraction.

Samples	2θ [°]	β= FWHM [°]	a_{200} $[\mathrm{A^{\circ}}]$	D_{200} [nm]	ε_{200} $\times 10^{-3}$
Pure NiO	43.192	0.898	4.1876	9.52	9.9
$\mathbf{Ni_{0.9}Cu_{0.1}O}$	43.07	1.212	4.199	7.05	13.4
$\mathbf{Ni_{0.9}Cu_{0.075}Zn_{0.025}O}$	43.09	1.122	4.1972	7.61	12.4
$\mathbf{Ni_{0.9}Cu_{0.05}Zn_{0.05}O}$	43.10	1.180	4.1962	7.23	13.04
$\mathbf{Ni_{0.9}Cu_{0.025}Zn_{0.075}O}$	43.02	0.953	4.2036	8.95	10.55
$\mathbf{Ni_{0.9}Zn_{0.1}O}$	42.997	0.831	4.2056	10.27	9.21

3.2 Optical properties

Absorbance measurements were performed for pure NiO and $\mathbf{Ni_{0.9}(Cu_{1-x}Zn_x)_{0.1}O}$ nanostructures at x= 0, 0.25, 0.5, 0.75 and 1 recorded in the wavelength range from 190 nm to 1100 nm. Fig 2a shows the change of the absorbance spectra as a function of the wavelength. Figure 2a shows the UV–Vis absorption spectra with the absorption peak of pure NiO at about 332 nm while, $\mathbf{Ni_{0.9}(Cu_{1-x}Zn_x)_{0.1}O}$ presente the absorption peaks at the range of (309 – 319 nm) that indicate to blue shift of the absorption peaks . Optical absorption data at x= 0 indicated strong absorption peaks shifted towards blue (to higher wavelength) with respect to the peak of undoped NiO NPs due to quantum confinement effect[10]. The blue shift of the absorption peaks occur because of Burstein–Moss effect, which confirm the quantum confinement effect [11]. In Figure 2b it can observed that the transmittance of pure NiO nanostructure reduces after the incorporation of the single and dual doped NiO nanostructures. The obtained transmittance was found to be about 85% for pure NiO while in the range (75 - 78%) of transmittance for

single and dual doped NiO nanostructures, this range located in the visible light spectra. This results are consistent with the previous studies [10, 11].

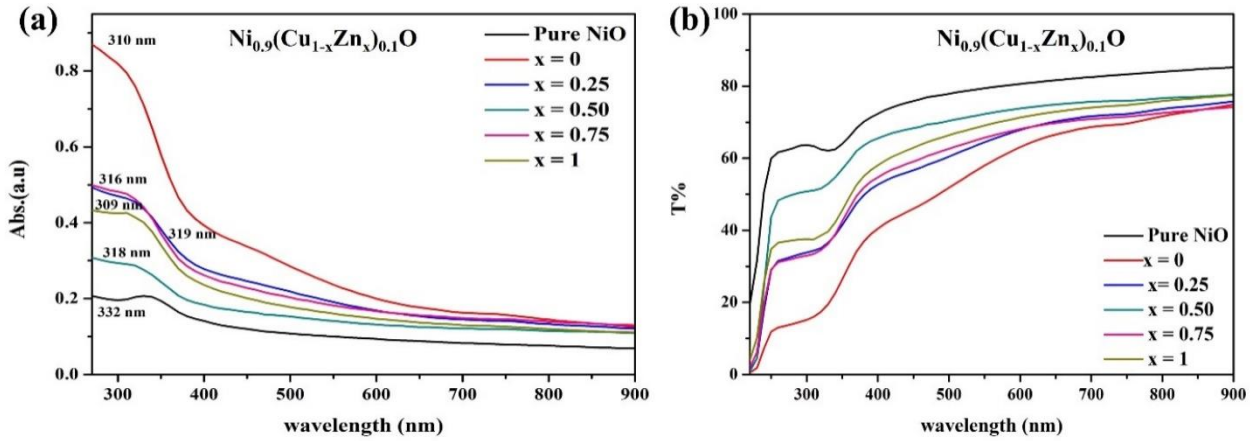

Figure 2. (a) Absorbance and (b) Transmittance spectra of undoped and doped NiO nanostructures.

The absorption coefficient (α) of the prepared samples can be calculated as follows [17]:

$$\boldsymbol{\alpha = 2.303\frac{A}{d}} \qquad (4)$$

Where (d) is the thickness of the sample cell and (A) is the measured absorbance by UV–Visible Spectrophotometer in as plotted in Figure 2a. The optical band gaps of samples have been calculated from Tauc's plot equation [18, 19] an extrapolation of the linear region of the plot $(\boldsymbol{\alpha h\upsilon})^{\boldsymbol{2}}$ versus energy $(\boldsymbol{h\upsilon})$ gives the optical bandgap value $\mathbf{E_g}$:

$$\boldsymbol{(\alpha h\upsilon)^2 = B(h\upsilon - E_g)} \qquad (5)$$

where $(\boldsymbol{h\upsilon})$ is the incident photon energy and (B) is a constant depending on the material. Figure 3a shows Tauc plot for pure NiO and $\mathbf{Ni_{0.9}(Cu_{1-x}Zn_x)_{0.1}O}$ at x= 0, 0.25, 0.5, 0.75 and 1. Bandgap energy of pure NiO is 3 eV which was in good agreement value with results that published by Alshahrie et.al., [20] and Hosny [21]. The single and dual doped NiO samples presents higher $\mathbf{E_g}$ values (3.22 – 3.18 eV) than pure samples as listed in Table 3. The results clearly indicate that the doping increased the band gap which indicated formation of smaller particle size due to quantum confinement effect that agree with Amita et.al., [22]. In general, the charge transfer from the O 2p states to the unoccupied Ni 3d states affected directly by the distortion of the $\mathbf{NiO_6}$ octahedra due to the increasing of dopant content [23]. The dopant occupation of the Ni sites indicates to reduce the nonlocal Zhang-Rice bound state, thus the band gap energy increase. The maximum change in bandgap of NiO were observed for $\mathbf{Ni_{0.9}Cu_{0.1}O}$ (3.22 eV) at x= 0.25.

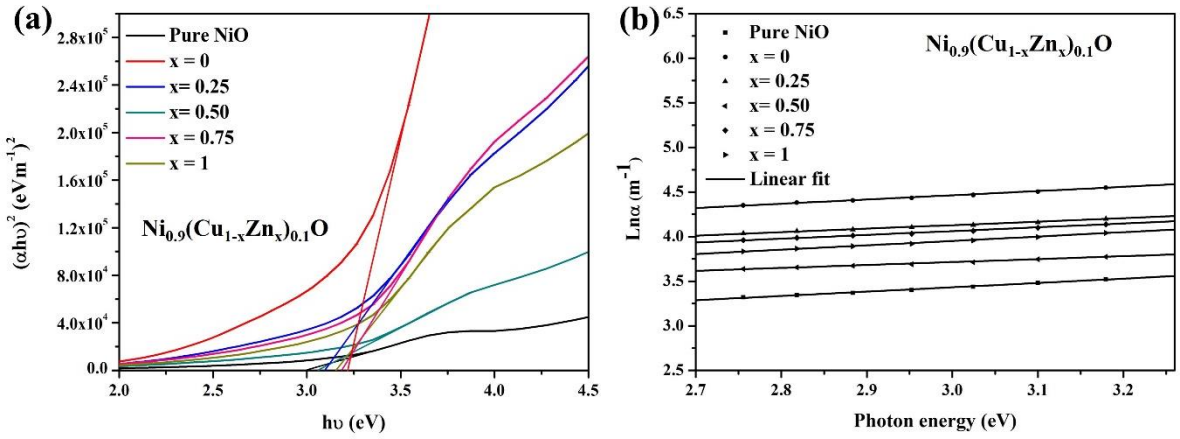

Figure 3. (a) Optical band gap energy (Eg) and inset shows the cut-off values on horizontal axis (photon energy axis). (b) Lnα versus E fitted to the best straight lines for the undoped and doped NiO nanostructures.

Table 3: The optical band gap and Urbach tail energies of prepared samples.

Samples	E_g [eV]	E_u [eV]
Pure NiO	3	2.06
$\mathbf{Ni_{0.9}Cu_{0.1}O}$	3.22	2.10
$\mathbf{Ni_{0.9}Cu_{0.075}Zn_{0.025}O}$	3.1	2.54
$\mathbf{Ni_{0.9}Cu_{0.05}Zn_{0.05}O}$	3.06	3.04
$\mathbf{Ni_{0.9}Cu_{0.025}Zn_{0.075}O}$	3.18	2.34
$\mathbf{Ni_{0.9}Zn_{0.1}O}$	3.16	2.04

The Urbach tail width calculated using equation [24, 25]:

$$\boldsymbol{\alpha = \alpha_0 exp\ (hv/E_u)} \qquad (6)$$

where $\boldsymbol{\alpha_0}$ is characteristic constant depends on materials. The plotting data of on y-axis versus corresponds to the exponential range (Urbach tail range) on x-axis explored a linear relation as shown in Figure 3b. The values were obtained for all prepared samples from the inverse of the slope values of the linear fit and listed in Table 3. Urbach tail energy $\mathbf{E_u}$ values followe the opposite behavior of band gap energy values because of the increase of the disorder and defect states with dopant [12]. The minimum value of $\mathbf{E_u}$ was 2.04 eV at x=1.

The refractive index (n) and absorption index (k) calculated from equation [24]:

$$\boldsymbol{k = \frac{\alpha\lambda}{4\pi}} \qquad (7)$$

$$n=\frac{1+R^{1/2}}{1-R^{1/2}} \quad (8)$$

Figure 4a shows the single and dual doped NiO NPs that indicated the higher refractive index at x= 0 and x= 0.75 respectively. Results presented that Cu dopants increased the refractive index due to higher polarization of Cu atoms in the NiO lattice matrix and in pure NiO sample was the lowest one indicated that NiO host lattice doesn't contain major defects [26]. The real and imaginary parts of the dielectric constant can be calculated from equation [27, 28]:

$$\boldsymbol{\varepsilon = \varepsilon_1 - i\varepsilon_2} \quad (9)$$

$$\varepsilon_1 = n^2 - k^2 \text{ and } \varepsilon_2 = 2nk \quad (10)$$

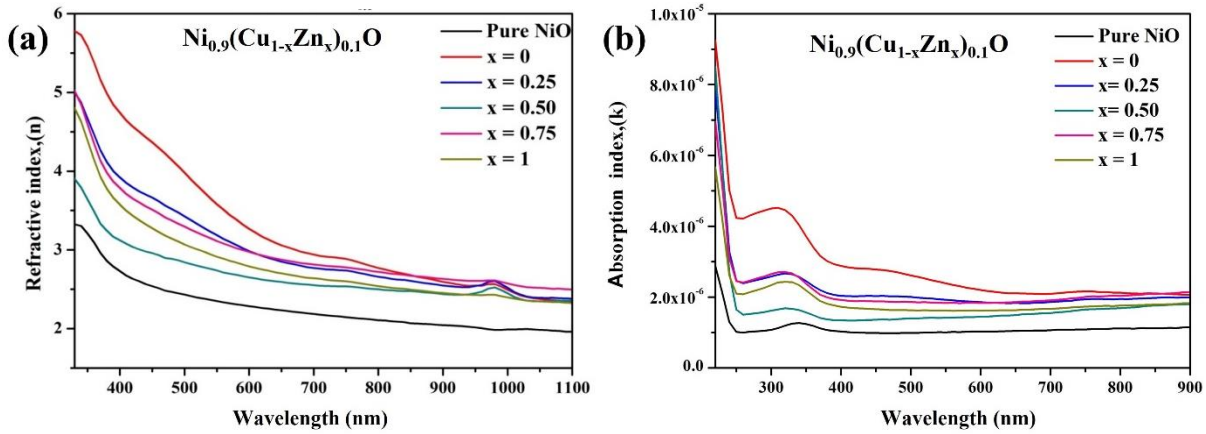

Figure 4. (a) Refractive index (n), and (b) Absorption index (k) of undoped and doped NiO nanostructures as a function of wavelength at different values of x.

The calculated values of $\boldsymbol{\varepsilon_1}$and $\boldsymbol{\varepsilon_2}$ as functions in the photon energy for prepared pure, single and dual doped NiO nanostructures are shown in Figure 5. From Figure 5a shows the calculate value of the real parts of the dielectric constant for samples between 11 s/m and 33.11 s/m in range~$\boldsymbol{3.7}$ **eV**. The single doped NiO at x= 0 (10 wt.% Cu and 0 wt.% Zn) and dual doped NiO at x= 0.75 (2.5 wt.% Cu and 7.5 wt.% Zn) obtained the higher values of dielectric constant. It can be observed that the value of real and the imaginary parts of dielectric increasing with increase doping.

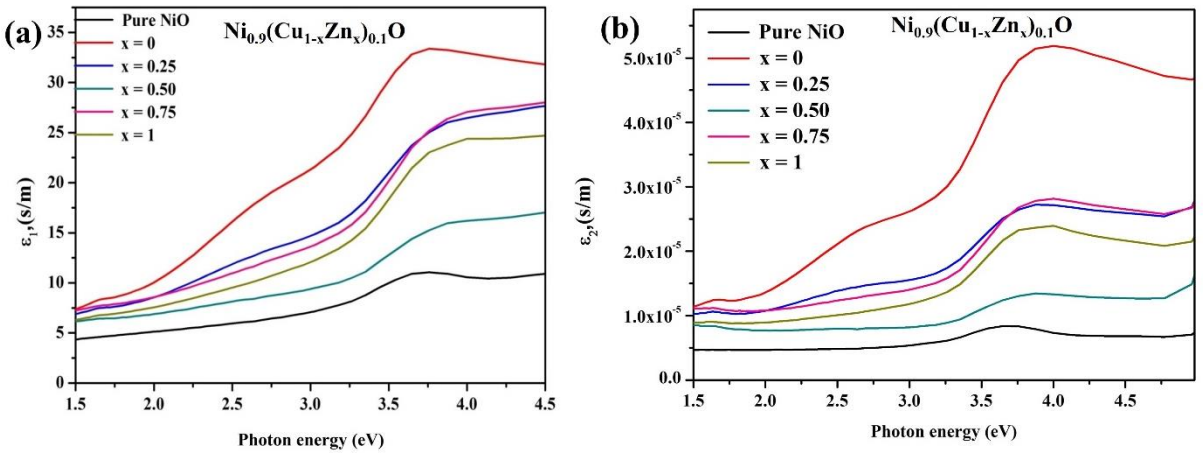

Figure 5. (a) The real ($\boldsymbol{\varepsilon_1}$) and imaginary ($\boldsymbol{\varepsilon_2}$) (b) parts of the dielectric constant on the photon energy for the undoped and doped NiO nanostructures.

Optical conductivity ($\boldsymbol{\sigma_{opt}}$) of the pure and doped NiO nanostructures can be calculated from equation[29]:

$$\boldsymbol{\sigma_{opt}} = \frac{\boldsymbol{\alpha n c}}{\boldsymbol{4\pi}} \qquad (11)$$

whereα, n and c are given by, absorption coefficient, refractive index and speed of light (3×10^8 m/s), respectively. In Figure 6 can observed that the optical conductivity increasing with increase photon energy for all samples. The prepared samples exhibited the maximum of σ_{opt} in range from 2.4×10^{10} to $3.6\times 10^{9}\ s^{-1}$ over ultraviolet region and minimum value in range 1.1×10^{10} to $2.6 \times 10^{9}\ s^{-1}$ over visible light region which approved that these samples preserve good photo response.

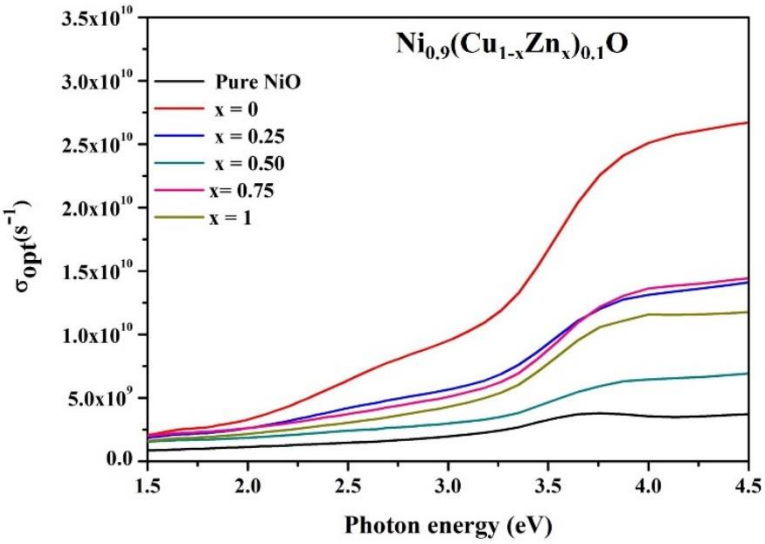

Figure 6. Optical conductivity on the photon energy for the undoped and doped NiO nanostructures.

3.3 DC electrical conductivity (σ_{dc})

Current-voltage measurements are in order to evaluate electrical properties of pure NiO, single and dual doped NiO nanostructures. The resistance (R) is obtaining from the I-V measurements. The DC electrical conductivity values was measured for all prepared samples using the following formula [30]:

$$\boldsymbol{\sigma_{dc}} = \frac{\mathbf{1}}{\mathbf{R}} \times \frac{\mathbf{l}}{\mathbf{A}} \qquad (12)$$

where R is the measured resistance, *A* is the cross-section area and ***l*** is the pellet thickness. σ_{dc} of NiO by I-V measurements is 3.70×10^{-5} S.cm^{-1} this result close from study Biju [31]. The DC electrical conductivity was affected by substitution of $Cu^{2+}$and Zn^{2+} in NiO crystal lattice that decrease from 1.620×10^{-4} S. cm^{-1} to 2.00×10^{-5} S. cm^{-1}. Figure 7 showed DC conductivity (σ_{dc}) and optical band gap energy (E_g) versus x values for pure NiO and$Ni_{0.9}(Cu_{1-x}Zn_x)_{0.1}O$.

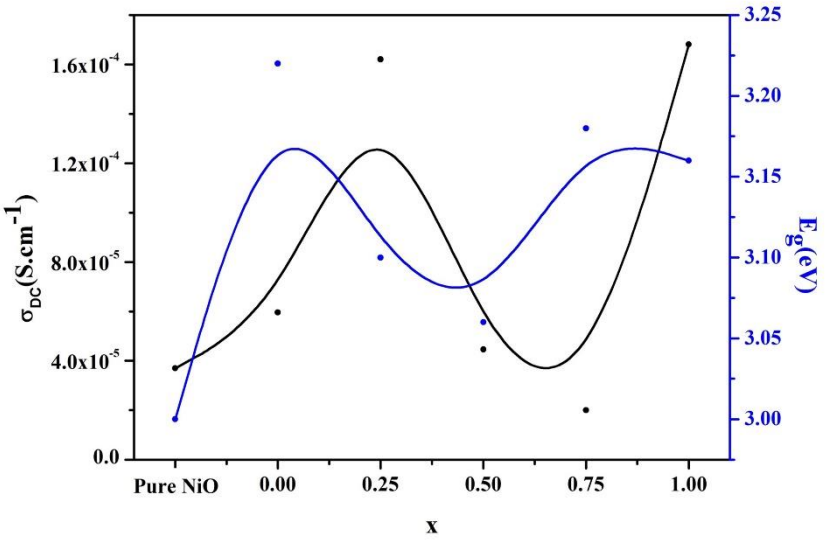

Figure7. DC electrical conductivity σ_{dc} of the NiO samples by I-V measurements versus band gap energy (Eg) as a function of x values. by I-V measurements.

4 Conclusions

Pure NiO, single and dual doped NiO nanostructures with x = 0, 2.5, 5, 7.5, and 10 wt% were successfully prepared by the co-precipitation method and annealed at 350 ℃ for 2 hours. The XRD patterns showed that the average value of crystallite size was between 7.05 and 10.27 nm. The addition of dopants increases the energy gap (E_g) from 3 eV for pure NiO. The maximum change in the band gap of NiO at x = 0.25 due to the occupation of Ni sites by the dopants indicates a decrease in the nonlocal Zhang-Rice bonding state, which increases the band gap energy. Due to the Cu and Zn cations causing substitutional defects in the NiO band gap, the dual doped NiO samples had lower σ_{dc} values than the single doped samples. Dual doped NiO nanostructures will exhibit novel improved properties when the concentration of metal dopants is changed, or these dopants are replaced by others in photoelectronic applications.

References

[1] Bonomo, M. (2018) Synthesis and characterization of NiO nanostructures: a review, *Journal of Nanoparticle Research* **20**: 222.

[2] Sayyadi, K., Gharani, M., Rahdar, A. (2019) The effect of solvent and temperature on the optical and structural properties of the nickel oxide and Cu-doped nickel oxide nanoparticles, *Advances in Nanochemistry* **1**: 34-40.

[3] Yousaf, S., Zulfiqar, S., Shahi, M.N., Warsi, M.F., Al-Khalli, N.F., Aboud, M.F.A., Shakir, I. (2020) Tuning the structural, optical and electrical properties of NiO nanoparticles prepared by wet chemical route, *Ceramics International* **46**: 3750-3758.

[4] Nakate, U.T., Lee, G.H., Ahmad, R., Patil, P., Bhopate, D.P., Hahn, Y., Yu, Y., Suh, E.-k. (2018) Hydrothermal synthesis of p-type nanocrystalline NiO nanoplates for high response and low concentration hydrogen gas sensor application, *Ceramics International* **44**: 15721-15729.

[5] Karthikeyan, M., Kumar, P.V., Ahamed, A.J., Ravikumar, A. (2020) Synthesis of Mg^{2+} doped NiO nanoparticles and their structural and optical properties by Co-precipitation method, *Journal of Advanced Applied Scientific Research-ISSN* **2454**: 3225.

[6] Ponnusamy, P., Agilan, S., Muthukumarasamy, N. (2015) A Simple route synthesis of Cr-doped NiO nanoparticles and their characterisation studies, *Int. J. Chem. Sci* **13**: 683-692.

[7] Mallick, P., Mishra, N. (2012) Evolution of structure, microstructure, electrical and magnetic properties of nickel oxide (NiO) with transition metal ion doping, *American Journal of Materials Science* **2**: 66-71.

[8] Mahmoud, S.A., Shereen, A., Mou'ad, A.T. (2011) Structural and optical dispersion characterisation of sprayed nickel oxide thin films, *Journal of modern Physics* **2**: 1178-1186.

[9] Rani, B.J., Ravi, G., Yuvakkumar, R., Ravichandran, S., Ameen, F., Al-Sabri, A. (2019) Efficient, highly stable Zn-doped NiO nanocluster electrocatalysts for electrochemical water splitting applications, *Journal of Sol-Gel Science and Technology* **89**: 500-510.

[10] Varunkumar, K., Ethiraj, A.S., Kechiantz, A. (2018) Optical absorption and thermal stability study of Cu doped NiO nanoparticles, AIP Conference Proceedings, AIP Publishing LLC, pp. 030174.

[11] Varunkumar, K., Hussain, R., Hegde, G., Ethiraj, A.S. (2017) Effect of calcination temperature on Cu doped NiO nanoparticles prepared via wet-chemical method: Structural, optical and morphological studies, *Materials science in semiconductor processing* **66**: 149-156.

[12] Al Boukhari, J., Zeidan, L., Khalaf, A., Awad, R. (2019) Synthesis, characterization, optical and magnetic properties of pure and Mn, Fe and Zn doped NiO nanoparticles, *Chemical Physics* **516**: 116-124.

[13] GangaReddy, K., Reddy, M.R. (2023) Physical vapour deposition of Zn^{2+} doped NiO nanostructured thin films for enhanced selective and sensitive ammonia sensing, *Materials Science in Semiconductor Processing* **154**: 107198.

[14] Sathishkumar, K., Shanmugam, N., Kannadasan, N., Cholan, S., Viruthagiri, G. (2015) Synthesis and characterization of Cu^{2+} doped NiO electrode for supercapacitor application, *Journal of Sol-Gel Science and Technology* **74**: 621-630.

[15] Lide, D. (2004) CRC Handbook of Chemistry and Physics, 85 ed., CRC Press, Boca Raton, pp. 2661.

[16] Thangamani, C., Pushpanathan, K. (2016) Optical and dielectric behavior of NiO: Zn quantum dots, *J Chem Pharm Res* **8**: 749-757.

[17] Ahmed, A.A.A., Al-Hesni, N.M., Al-Osta, A.H., Al-Salmi, M.L., Manssor, K.A., Saleh, M., Al-Asbahi, B.A., Qaid, S.M., Ghaithan, H.M., Farooq, W. (2021) Influence of single and dual doping (Ag and Co) on the optical properties of CdS quantum dot thin films for solar application, *Optik* **246**: 167824.

[18] Al-Mushki, A.A., Ahmed, A.A.A., Abdulwahab, A., Al-Asbahi, B.A., Abduljalil, J.M., Saad, F.A., Al-Hada, N.M., Qaid, S.M., Ghaithan, H.M. (2022) Structural, optical, and antibacterial characteristics of mixed metal oxide CdO–NiO–Fe_2O_3 nanocomposites prepared using a self-combustion method at different polyvinyl alcohol concentrations, *Applied Physics A* **128**: 279.

[19] Ahmed, A.A.A., Al-Mushki, A.A., Al-Asbahi, B.A., Abdulwahab, A., Abduljalil, J.M., Saad, F.A., Qaid, S.M., Ghaithan, H.M., Farooq, W., Omar, A.-E.H. (2021) Effect of ethylene glycol concentration on the structural and optical properties of multimetal oxide CdO–NiO–Fe_2O_3 nanocomposites for antibacterial activity, *Journal of Physics and Chemistry of Solids* **155**: 110113.

[20] Alshahrie, A., Yahia, I., Alghamdi, A., Al Hassan, P. (2016) Morphological, structural and optical dispersion parameters of Cd-doped NiO nanostructure thin film, *Optik* **127**: 5105-5109.

[21] Hosny, N.M. (2011) Synthesis, characterization and optical band gap of NiO nanoparticles derived from anthranilic acid precursors via a thermal decomposition route, *Polyhedron* **30**: 470-476.

[22] Amita, Deepak, Arun, Rana, P.S. (2019) Synthesis, characterization and sunlight catalytic performance of Cu doped NiO nanoparticles, AIP Conference Proceedings, AIP Publishing LLC, pp. 020035.

[23] Sawatzky, G., Allen, J. (1984) Magnitude and origin of the band gap in NiO, *Physical review letters* **53**: 2339.

[24] Ahmed, A.A.A., Abdulwahab, A., Talib, Z.A., Salah, D., Flaifel, M.H. (2020) Magnetic and optical properties of synthesized ZnO–$ZnFe_2O_4$ nanocomposites via calcined Zn–Fe layered double hydroxide, *Optical Materials* **108**: 110179.

[25] Ahmed, A.A.A., Al-Hussam, A.M., Abdulwahab, A.M., Ahmed, A.N.A.A. (2018) The impact of sodium chloride as dopant on optical and electrical properties of polyvinyl alcohol, *AIMS Materials Science* **5**: 533-542.

[26] Shkir, M., Arif, M., Ganesh, V., Singh, A., Algarni, H., Yahia, I., AlFaify, S. (2020) An effect of Fe on physical properties of nanostructured NiO thin films for nonlinear optoelectronic applications, *Applied Physics A* **126**: 119.

[27] Mandrić Radivojević, V., Rupčić, S., Srnović, M., Benšić, G. (2018) Measuring the dielectric constant of paper using a parallel plate capacitor, *International journal of electrical and computer engineering systems* **9**: 1-10.

[28] Fox, M. (2001) Interband absorption in, *Optical Properties of Solids* 49-75.

[29] Hassanien, A.S., Akl, A.A. (2015) Influence of composition on optical and dispersion parameters of thermally evaporated non-crystalline Cd50S50− xSex thin films, *Journal of Alloys and Compounds* **648**: 280-290.

[30] Popescu, I., Skoufa, Z., Heracleous, E., Lemonidou, A., Marcu, I.-C. (2015) A study by electrical conductivity measurements of the semiconductive and redox properties of Nb-doped NiO catalysts in correlation with the oxidative dehydrogenation of ethane, *Physical Chemistry Chemical Physics* **17**: 8138-8147.

[31] Biju, V., Khadar, M.A. (2001) DC conductivity of consolidated nanoparticles of NiO, *Materials research bulletin* **36**: 21-33.

Thamar University Journal of
Natural & Applied Sciences

TuJNAS

ISSN-Print: 2073-0764
ISSN-Online: 2959-4340

Volume 8, Issue 1, 2023

CONTENTS

Papers

Thamar University Publications